Rate-based modeling approach for High Pressure Water Scrubbing with unsteady gas flowrate and multicomponent absorption applied to biogas upgrading

Eliot Wantz, David Benizri, Gilles Hébrard, N. Dietrich

Rate-based modeling approach for High Pressure Water Scrubbing with unsteady gas flowrate and multicomponent absorption applied to biogas upgrading

Eliot Wantz[1], David Bénizri[2], Nicolas Dietrich[1], Gilles Hébrard[1,*]

[1] *TBI, Université de Toulouse, CNRS, INRA, INSA, Toulouse, France*

[2] *Epurtek, SAS, 81 Chemin de Mange-Pommes, 31520 Ramonville-Saint-Agne, France*

*Corresponding author: gilles.hebrard@insa-toulouse.fr (G. Hébrard)

Highlights

- An innovative rate-based model for HPWS is proposed applied to biogas upgrading
- The model considers gas flowrate decrease and concomitant absorption of CO_2 and CH_4
- Modeling of mass transfer and driving force is possible all along the column height
- CH_4 purity and recovery of data collected on a farm biogas plant are accurately predicted
- Operating conditions are assessed to optimize HPWS performances and power requirement
- Water regeneration increases CH_4 purity over 97 % and its recovery to 93 %

Abstract

Biogas upgrading aims to increase methane concentration in biogas by removing carbon dioxide. Upgraded biogas can therefore be used as renewable energy resource. Among the different technologies used for biogas upgrading, High Pressure Water Scrubbing (HPWS) is one of the most widespread. HPWS is identified to fulfill all the requirement for farm-scale anaerobic digester, presenting several levers to reduce operational and installation costs. A possible remedy is to optimize operating parameters to reach targeted gas specifications, without applying excessive treatment and energy consumption. The purpose of this study is to develop an efficient modeling tool that can predict methane purity and its recovery for different operating conditions of gas and liquid. This original model integrates gas flow decrease along the packing height and concomitant absorption of carbon dioxide and methane. The model is based on mass transfer and hydrodynamics to enlighten and anticipate performance of HPWS in order to facilitate its implementation on the field. Modeled results are compared to experiments conducted on a farm-scale biogas upgrading plant. Modeled results are in great agreements with the experimental results and the model shows a great adaptability regarding the parameters variations. It can therefore be used to

anticipate HPWS performances and to optimize running parameters to reach targeted purities while loosening energy consumptions. Water regeneration was identified to be the key parameter to comply with gas injection standards, achieving a purity over 97 % and a recovery ratio of 93 % at a desorption pressure of 0.2 bar. Results highlight that a rate-based model giving access to molar fraction variation along the column is crucial to adjust operating parameters in order to reach optimal economical and environmental performances. More accurate operating conditions could be the key to withstand low costs of production and to meet financial viability for biogas upgrading at farm-scale.

Keywords

Biogas Upgrading, High Pressure Water Scrubbing, Mass Transfer, Rate-based modeling, Process Simulation, Renewable Energy

Graphical Abstract

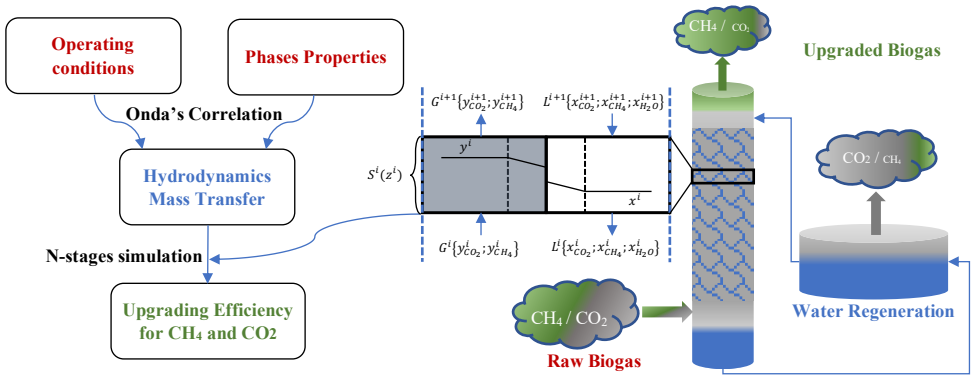

1 Introduction

Energy is one of a key factor associated to the development of human societies. It is closely linked to the history of successive civilizations and it is now more than ever a founding principle of human living conditions [1]. But the intense consumption of fossil energy resources has led to environmental issues with worrying prospect for the future [2]. A possible remedy was found in the energy transition, involving among others routes to substitute the fossil fuels by renewable fuels [3]. One of those renewable energies that has great chance to spread in a near future is biogas, as it is a local, universal and sustainable energy [4,5].

Biogas is produced mostly by anaerobic digestion of organic matter. It is composed of methane (from 50 to 80 % in volume) and carbon dioxide (from 50 to 30 % in volume) together with several impurities (such as hydrogen

sulfide) [6]. Its composition depends on the origin of the matter and the plant type associated (e.g. agricultural wastes, manure, or food industry by-products). Even tough biogas is primarily used to produce electricity and heat by cogeneration, some drawbacks of this technic (weak electrical yield, maintenance costs, inefficient heat valorization) leads to develop other pathways for biogas recovery [5,7–9]. It is essentially about meeting natural gas standards by increasing methane concentration – called biogas upgrading. Required methane purity varies upon the countries' standards, but it is generally around 97 %. Biomethane can therefore be used as vehicle fuel or in substitution to the natural gas in gas mains [9–11].

A great diversity of technologies was investigated for biogas upgrading. The most widespread are Pressure Swing Adsorption, Membranes Separation, Cryogenic Upgrading, and Absorption Process (only physical absorption or involving chemical reaction) [10–12]. If most of those technics are mature for large biogas plant (in majority over 100 Nm^3/h of biogas flowrate), they are not viable anymore for smaller anaerobic digester, typically bellow 40 Nm^3/h of biogas production [8,13,14]. It is indeed necessary to maintain the same level of control on both the small and large biogas plant, including sensor, valves, and automation. But it is more and more accepted that small biogas plants are best suited to this production, mostly regarding the distribution of the biomass that is scattered all around territories [8,15]. Those process also suffers from some drawbacks, such as methane leaks in the off-gas, excessive power requirements to achieve a desired biogas upgrading, or an unoptimized integration of the process in the valorization path [16–18]. This makes Wilhelm Ostwald thought "Do not waste energy, make it useful" relevant for the optimization of the biogas valorization [1]. Great improvements can therefore be proposed on biogas upgrading to loosen investment and operating costs to maximize the energy return on investment and the financial viability of this new industry [5,18,19]. As suggested by Sahota et al. (2018), one lever is to simplify the technology to reduce investment and operating costs [14]. This involves to optimize every operation of the process, but also to have available a precise modeling tool to anticipate the process performances and optimize the energy consumption [5,20,21].

High Pressure Water Scrubber (HPWS), an absorption process, have been identified to meet the requirement for both purification efficiency and possibility to simplify the technology [14,22]. It is a frugal and solid device suited for agricultural environment, easily adaptable between different unit. Several studies compare cost analysis between technologies applied in biogas upgrading, and HPWS appeared to be one of the most economical methods [19,23]. But in order to reduce environmental impact, it has to be conducted with regeneration of the liquid phase to avoid water depletion and without any addition of chemical compounds. Thus, it is conducted with water in closed loop. In this configuration, main energy consumption is due to water pumping and gas compression [10].

Also, in order to insure optimum financial viability, it is crucial that the upgraded biogas meet the required specification to avoid non-compliance situation and so financial losses. A minimal energy consumption set to meet the standards without any over-treatment, allowing a full-time gas compliance, is the key to go over the break-even point and to maximize the methane recovery [16,24,25]. To meet these conditions, a precise knowledge on absorption efficiencies have to be developed, depending on operating parameters such as the gas and liquid flowrate, their composition, the working pressure, or the temperature. Modeling of HPWS appears to be an efficient tool to meet optimum operating conditions and to adapt HPWS on various biogas production. But as pointed out by several authors, there is a lack of simulations studies and modeling methods to optimally conduct HPWS [16,24,26]. A need to go further in those methods is necessary to find optimum operational conditions regarding absorption efficiency and environmental footprint [27,28].

HPWS is usually conducted in packed column, encouraging contact between phases and promoting mass transfer [29]. Packed columns are largely studied worldwide, in terms of hydrodynamics, packing optimization, and absorption efficiency, leading to various modeling methods based either on equilibrium stages or on mass transfer rate [29,30]. The rate-based model using Unit Transfer is constructed on the combination of both mass transfer phenomenon and flow modeling, including hydrodynamics in the column. It is better suited for scale-up and adaptability as it is considering these variabilities [29,30]. The model was tested in most common cases complying with the following hypothesis: a steady gas flowrate all along the packing height and a packing height sufficient to achieve the equilibrium between the gas and the liquid at the bottom of the column. Those hypotheses are acceptable in most cases, when the targeted component is diluted in the gas stream. But for biogas upgrading, the gas flowrate is reduced from around 50 % between the inlet and the outlet and the packing height is not always correlated to an equilibrium at the bottom of the column, leading to questionable hypothesis [15]. Significant methane losses are also reported in the literature due to gas dissolving in the liquid [13,16]. It is therefore a concomitant carbon dioxide and methane absorption situation that must be considered for a relevant modeling. However, it is not always considered in the modeling methods encountered [20,24,26]. Such a model can not be found in the literature, gathering rate-based hypothesis, gas flow reduction and concomitant carbon dioxide and methane absorption.

The main goal of the present study is to propose an original adaptation of the Unit Transfer modeling to multicomponent rich gas absorption, considering gas flowrate variations along the column. The context of biogas upgrading is taken as a reference to evaluate the model. Modeled results of methane purity and its recovery are compared to experimental data collected on a full-scale HPWS demonstrator set up on a farm biogas plant for

validation. Model is then used to evaluate the mass transfer parameters evolution into the column and the parameters influence (such as the working pressure in the column, the temperature, the gas and liquid flowrates, the packing material or the water regeneration) on the process performances. The objective is to better understand every parameters impact in order to choose the optimal set of value to reach desired methane purity while limiting methane leaks, minimizing energy consumption, and so improving biogas upgrading efficiency and viability.

2 Experimental Methods

2.1 Process Operation

HPWS used in this study is a random packed tower working in closed loop with water as liquid phase. It is the same configuration as the one used by Bénizri et al. (2019) [13]. Figure 1 presents the flowsheet of the HPWS used in this study.

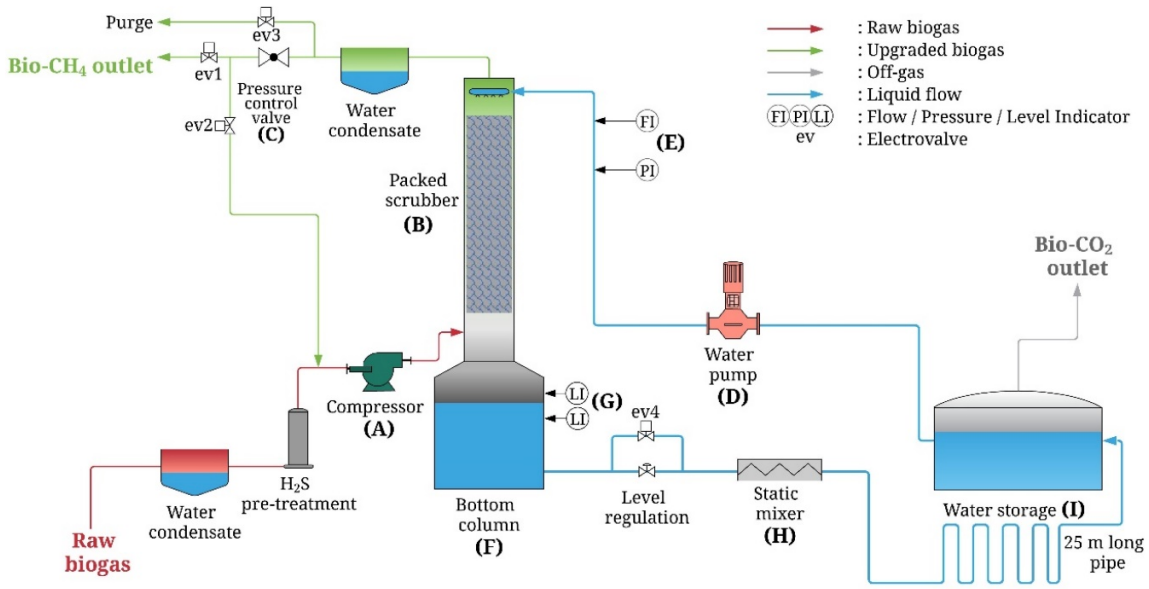

Figure 1: Flow diagram of the biogas upgrading plant

Raw biogas is extracted from the digester and cooled down at ambient temperature. Water condensate are collected and evacuated using a water drain. A pretreatment containing iron filings is then set to remove H_2S ($\leq$ 300 ppm) from the biogas. Biogas is then compressed (A) and fed into the packed scrubber. The gas rises to the top of the column, meeting through the random packing (B) the liquid flowing down in counter-current. Upgraded biogas is recovered at the top of the column through a pressure regulation valve (C) (set at desired pressure, e.g. 5 to 10 bars).

Water is injected at the top of the column (E) with a water pump (D) through a perforated sparger. Water saturated in gas at the bottom of the column (F) is released at atmospheric pressure by a motorized valve. Water level is measured by vibrating level switch (G) (Bürkert level switch 8111) and regulated by a manual diaphragm valve (adjusted for a known couple of pressure-flow) associated to a motorized valve. Compressor (Mauguières MRL100-10) and water pump (Salmson MultiV800) are frequency driven by an industrial computer. Random packing used in this study is RaschigSuperRing® from Raschig GmbH, made of Polypropylene to withstand the aggressive environment. Characteristics of the packing material are reported in Table 1.

Table 1: Packing characteristics

Packing Type	**d_P (m)**	**a^* (m^2/m^3)**	**F (m^2/m^3)**	**ε_g**	**N (m^{-3})**	**ρ ($kg.m^{-3}$)**	**σ ($N.m^{-1}$)**
RaschigSuperRing® (PP)	0.05	250	180	0.93	60000	62	0.04

Bottom column (B) presents a wider diameter (D_{bottom} = 0.5 m) than the column (D_{col} = 0.26 m) itself to prevent biogas leaks, as patented by Hébrard et al. (2014) [31]. This avoids microbubbles of biogas to be dragged down by the liquid flow by diminishing its velocity.

Water regeneration is conducted using a new method including a static mixer (H), as patented by Hébrard et al. (2011) [32]. Static mixer promotes gas desorption. The multiphase flow generated circulates through a 25 m long pipe where gas bubble coalescence occurs and the flow stratifies. Gas phase is separated from the liquid in a storage tank (I) (1.2 m^3 capacity), and the regenerated water is pumped to the column for a new absorption cycle.

Water pipes are made of stainless steel and polyvinyl chloride, and gas pipes are stainless steel only. Top of the column is made of high-density polyethylene such as the storage tank, and bottom of the column is made of iron metal protected from corrosion by epoxy paint. Maximum admitted pressure is 16 bars for the pressurized part (only 10 bars reachable with the compressor). Maximum liquid flowrate is set at 10 m^3/h and gas flow at 40 Nm^3/h.

2.2 Analysis material

Water vapor is eliminated from the gas using a Peltier cooler (Herrmann Moritz) and a 200-micrometer filter. Gas flow and pressure are regulated before drying and analysis. Gas analysis is performed on a specific biogas equipment (BioBasic from Fresenius company) using infrared analysis for methane and carbon dioxide and electrochemical cells for hydrogen, oxygen, and hydrogen sulfide. Liquid flowmeter is a turbine-type from Kobold (DRB series). Pressure is measured by an Endress Hauser sensor (Cerabar PTP31). Gas flowrate at the outlet is

measured by a gas meter from Gurtner (G25). At the inlet of the column, compressor frequencies were calibrated to corresponding volumetric flow values.

3 Numerical Methods

Numerical methods are well developed in literature for most current cases of gas treatment, e.g. with lean gases. Those methods are based either on equilibrium consideration or in rate-based approach [29]. Equilibrium considerations are preferred in many cases, mostly with process simulation software, as it is easier in the calculation method. But for biogas upgrading, no analytical solution can be found for the rate-based approach as the volumetric gas flowrate can not be considered equal between the inlet and the outlet [29]. Simulation are thus usually conducted using equilibrium-based methods, the theoretical minimum stages number being determined by preliminary runs compared with an experimental database of the on-site process [17,25,26,33]. This required to have available those data to calculate *a posteriori* this stage number. In addition, a change in the operating conditions can lead to modifications in the hydrodynamics and the equilibrium prospect. For those reasons, equilibrium-based methods are not well suited to anticipate process performances on-site and for sizing purpose [20,24,29,33]. The model developed in this work is a rate-based approach that aims to free from the steady gas flowrate assumption.

3.1 Minimum liquid gas ratio

First is to determine the minimum liquid flowrate to establish at the inlet L_{min}^{in} in order to achieve the desired outlet gas composition in carbon dioxide and methane $\left\{y_{CO_2}^{out}; y_{CH_4}^{out}\right\}$ [30]. $L_{min}^{in}$is calculated using partial molar balance for carbon dioxide and methane (Equation (1) and (2)) and total molar balance (Equation (3)) between the inlet and the outlet. Water transfer to the gas phase is neglected.

$$y_{CO_2}^{in} G^{in} + x_{CO_2}^{in} L^{in} = y_{CO_2}^{out} G^{out} + x_{CO_2}^{out} L^{out} \quad (1)$$

$$y_{CH_4}^{in} G^{in} + x_{CH_4}^{in} L^{in} = y_{CH_4}^{out} G^{out} + x_{CH_4}^{out} L^{out} \quad (2)$$

$$G^{in} + L^{in} = G^{out} + L^{out} \quad (3)$$

In Equation (1), (2) and (3), $G^{in(out)}$ is the gas molar flowrate at the inlet (the outlet) of the column, $L^{in(out)}$ is the liquid molar flowrate at the inlet (the outlet) of the column, $x_i^{in(out)}$ is the molar fraction in the liquid at the inlet (the outlet) of compound *i* and $y_i^{in(out)}$ is the molar fraction in the gas at the inlet (the outlet) of compound *i*.

Considering that the liquid flowrate at the inlet is L_{min}^{in}, gas liquid equilibrium is assumed at the bottom of the column. Henry's law (Equation (4) and (5)) can be applied [34].

$$y_{CO_2}^{in} = H_{Co_2} x_{CO_2}^{out} = \frac{m_{Co_2}}{P} x_{CO_2}^{out} \quad (4)$$

$$y_{CH_4}^{in} = H_{CH_4} x_{CH_4}^{out} = \frac{m_{CH_4}}{P} x_{CH_4}^{out} \quad (5)$$

In Equation (4) and (5), H_i is the dimensionless partition coefficient of compound i and m_i is the partition coefficient in Pascals of compound i. Calco-carbonic phenomenon are neglected as carbonic acid is supposed to be the predominant specie, pH of the liquid rapidly acidifying to 5 [15,20,35].

The objective is to determine L to achieve a known couple $\{y_{CO_2}^{out}; y_{CH_4}^{out}\}$. G^{out} is expressed in Equation (6) as a function of L^{in}, summing Equation (1) and (2) and substituting L^{out} with Equation (3). It is also assumed that gas phase is only composed of carbon dioxide and methane (sums of the molar fraction are equal to 1 at the inlet and the outlet). x_i^{out} are substituted using Equation (4) and (5).

$$G^{out} = \frac{G^{in} + \left(x_{CO_2}^{in} + x_{CH_4}^{in}\right) L^{in} - \left(\frac{y_{CO_2}^{in}}{H_{CO_2}} + \frac{y_{CH_4}^{in}}{H_{CH_4}}\right)\left(G^{in} + L^{in}\right)}{1 - \left(\frac{y_{CO_2}^{in}}{H_{CO_2}} + \frac{y_{CH_4}^{in}}{H_{CH_4}}\right)} = f(L^{in}) \quad (6)$$

Molar fractions are calculated using Equation (7) by substituting G^{out} in Equation (1) and (2) by the expression obtained Equation (6).

$$y_j^{out} = \frac{\left(y_j^{in} G^{in} + x_j^{in} L^{in} - x_j^{out}\left(G^{in} + L^{in} - f(L^{in})\right)\right)}{f(L^{in})} \quad (7)$$

In this condition, an infinitely deep packed tower is necessary to achieve equilibrium. Liquid flowrate is then taken higher than the minimum liquid flowrate, generally between 1.2 and 1.4 [29]. This method allows to calculate the minimum liquid flowrate making no assumptions on a constant gas flowrate from the bottom to the top of the column, but it supposed that the gas liquid equilibrium is achieved.

3.2 Packing Height

Next step to design packed tower is to estimate height of the packing material. Among the different methods developed in the literature, the Unit Transfer concept is more suited for extrapolation as it considers hydrodynamics inside the column through mass transfer coefficient. Main limit of this method is that an analytical solution to the mass transfer equation can only be proposed by assuming a constant gas flowrate between the bottom and the top

of the column, namely for a lean-phase system. When talking of absorption from rich gases, where total gas flow decreases rising up the column, no obvious solution can be proposed to solve the equations, especially as two components are transferred to the liquid for biogas upgrading which makes it a multicomponent absorption system for rich gases [36].

In this method, the entire height of the packing material Z is divided in N-stages for discretization. On each stage, a steady gas flowrate is assumed between the inlet and the outlet of the stage, as presented in Figure 2. In this way, Unit Transfer method can be applied on each single stage.

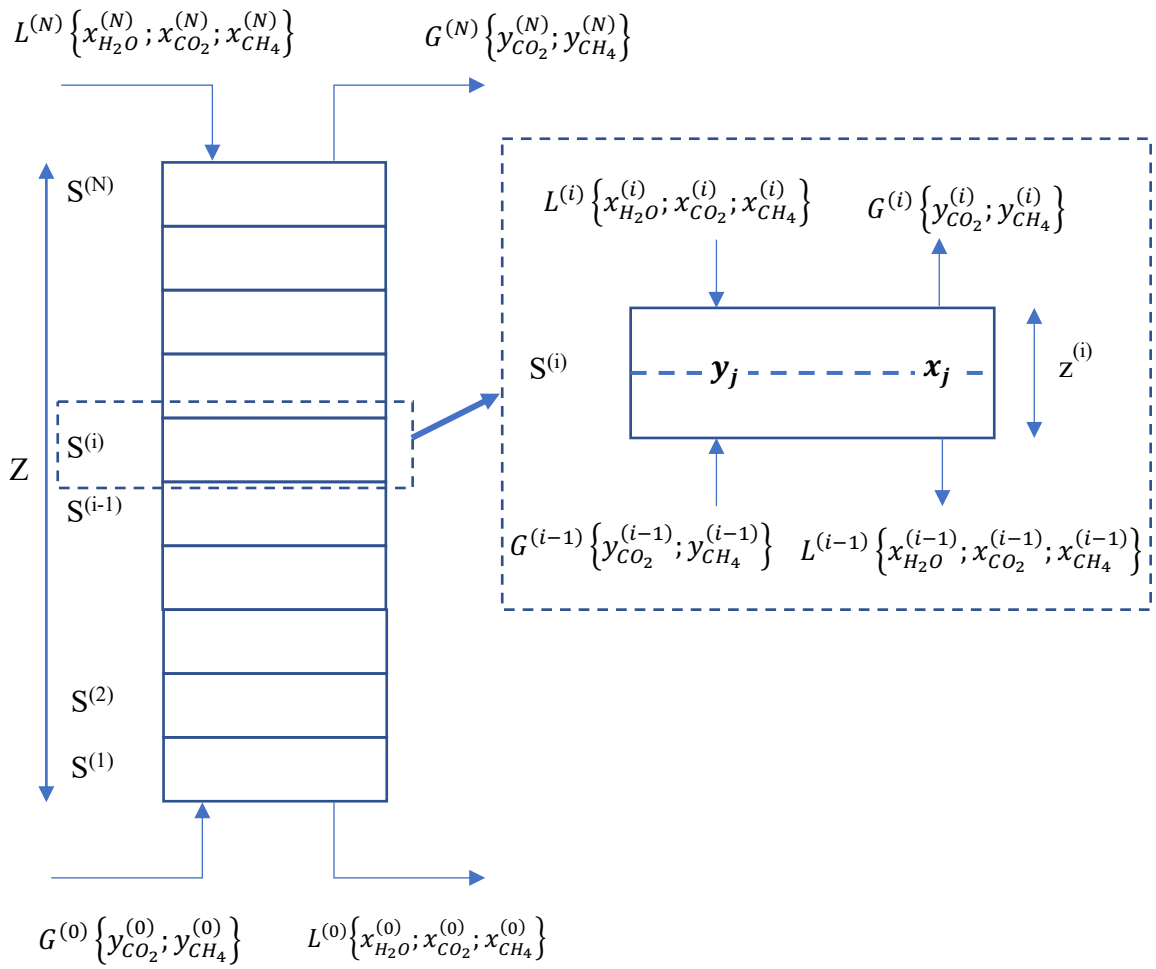

Figure 2: Multistage HPWS discretization.

Height $z^{(i)}$ of a single stage $S^{(i)}$ is calculated using Equation (8), where $HUT_j^{(i)}$ is the Height of a Unit Transfer in $S^{(i)}$ for compound j and $NUT_j^{(i)}$ is the Number of Unit Transfer in $S^{(i)}$ for compound j, respectively given using Equation (9) and (10). Those equations are derivated from the Lewis and Whitman model [29,37].

$$z^{(i)} = HUT_j^{(i)} \cdot NUT_j^{(i)} \qquad (8)$$

$$HUT_j^{(i)} = \frac{G^{(i-1)}}{K_{G,j}^{0,(i-1)} \cdot a^{0,(i-1)} \cdot \Omega} \quad (9)$$

$$NUT_j^{(i)} = \int_{y_j^{(i)}}^{y_j^{(i-1)}} \frac{dy_j}{y_j - y_j^*} \quad (10)$$

$K_{G,j}^{0,(i)}$ is the overall transfer coefficient for gas phase of compound j in $S^{(i)}$, $a^{0,(i)}$ is the area of interface per unit packed volume in $S^{(i)}$, Ω is the cross-sectional area of the column, and y_j^* j molar fraction in the gas phase in equilibrium with the liquid phase.

An analytical solution is proposed to calculate $NUT_j^{(i)}$, assuming steady gas and liquid molar flowrate on each stage. Molar balance applied to stage $S^{(i)}$ gives an expression for y_j, Equation (11), and y_j^* is defined by Equation (12).

$$y_j = \left(x_j - x_j^{(i)}\right)\left(\frac{L^{(i-1)}}{G^{(i-1)}}\right) + y_j^{(i)} \quad (11)$$

$$y_j^* = H_j x_j \quad (12)$$

y_j and y_j^* are substituted in Equation (10) using Equation (11) and (12), and integral calculus between $x_j^{(i)}$ and $x_j^{(i-1)}$ gives an expression of $NUT_j^{(i)}$ reported in Equation (13). The detail development that led to Equation (13) is proposed in **Erreur ! Source du renvoi introuvable.**.

$$NUT_j^{(i)} = \frac{A_j^{(i-1)}}{A_j^{(i-1)} - 1} \cdot \ln\left(\frac{y_j^{(i-1)} - H_j x_j^{(i-1)}}{\frac{A_j^{(i-1)} - 1}{A_j^{(i-1)}} y_j^{(i)} + \frac{y_j^{(i-1)}}{A_j^{(i-1)}} - H_j x_j^{(i-1)}}\right) \quad (13)$$

In Equation (13), A is the absorption factor defined in Equation (14).

$$A_j^{(i)} = \frac{L^{(i)}}{H_j \cdot G^{(i)}} \quad (14)$$

$K_{G,j}^{0,(i-1)}$ is calculated in $HUT_j^{(i)}$ using Equation (15), with k_G^0 and k_l^0 the mass transfer coefficient respectively for the gas phase and the liquid phase, calculated using Onda's correlation for k_L (Equation (17)) and k_G is calculated using Sherwood number Sh Equation (18) [38,39]. k^0 is related to k with Equation (16) [29].

$$\frac{1}{K_G^0} = \frac{1}{k_G^0} + \frac{H}{k_l^0} \quad (15)$$

$$k^0 = k \cdot \frac{\rho}{M} \quad (16)$$

$$k_L \cdot \left(\frac{\rho_L}{\mu_L \cdot g}\right)^{1/3} = 0.0051 \cdot \left(a^* \cdot d_p\right)^{-0.27} \cdot \left(\frac{a^0}{a^*}\right)^{-2/3} \cdot Re_L^{2/3} \cdot Sc_L^{-0.50} \quad (17)$$

$$k_G = \frac{Sh_G \cdot D_G}{d_p} \quad (18)$$

Where ρ_L is the volumetric mass density of the liquid, M the molecular weight, μ_L the viscosity of the liquid, g the gravitational acceleration, a^* the wetted surface area, d_p the diameter of a packing unit, Re the Reynolds Number, Sc the Schmidt Number, and D_G the diffusivity in the gas. All the dimensionless numbers are defined in the Symbols section.

Sherwood number is calculated using Equation (19), and the wetted surface area using Onda's correlation Equation (20) [39].

$$Sh_G = 5.23 \cdot \left(a^* \cdot d_p\right)^{-1.7} \cdot Re_G^{0.7} \cdot Sc_G^{1/3} \quad (19)$$

$$\frac{a^0}{a^*} = 1 - \exp\left(-1.45 \cdot \left(\frac{\sigma_c}{\sigma_L}\right)^{0.75} \cdot \left(a^* \cdot d_p\right)^{-0.35} \cdot Ga_L^{0.05} \cdot We_L^{0.2}\right) \quad (20)$$

σ is the surface tension, We the Weber number, and Ga the Galilei number.

For a given height of packing $z^{(i)}$, $HUT_j^{(i)}$ is calculated for both carbon dioxide and methane, using Equation (9). $NUT_j^{(i)}$ value is then taken from Equation (8), and $y_j^{(i)}$ is obtained with Equation (13).

Gas flow is adjusted at the outlet of stage $S^{(i)}$ (Equation (21)) by removing the quantity transferred to the liquid phase, and the liquid flow at the inlet is obtained with a mass balance (Equation (3)), such as the fraction of solute in the liquid phase (Equation (1) and (2)).

$$G^{(i)} = \left(y_{CO_2}^{(i)} + y_{CH_4}^{(i)}\right) \cdot G^{(i-1)} \quad (21)$$

$y_j^{(i)}$ to inject in the upper stage S^{i+1} is also adjusted ($y_j^{(i)}(adj)$) for both carbon dioxide and methane to take into account the transfer performed in stage S^i using Equation (22) in respect to Dalton's law.

$$y_{CO_2}^{(i)}(adj) = \frac{y_{CO_2}^{(i)}}{y_{CO_2}^{(i)} + y_{CH_4}^{(i)}} \; and \; y_{CH_4}^{(i)}(adj) = \frac{y_{CH_4}^{(i)}}{y_{CH_4}^{(i)} + y_{CO_2}^{(i)}} \quad (22)$$

Those adjustments on the gas fraction and the gas flowrate are possible only if the variations between $G^{(i)}$ and $G^{(i+1)}$ are small, which means that the number of stages N is sufficient. After preliminary runs, the number of stages was set at 120 for the three-meters packing height, allowing a volumetric gas flowrate decrease below 0.5 %.

3.3 Flash tank modeling

As industrial HPWS are working in closed loop on the water to prevent excessive water catchment, modeling of the absorption in the column is coupled with the regeneration unit. In the process considered in this work, the gas is separated from the water using a static mixer to promote gas desorption, and a separation tank at atmospheric pressure associated to a 25 meters long pipe to stratified and separate the gas and the liquid. This configuration can be substituted by a classical flash tank presented Figure 3. Outlet flows can be calculated considering that the equilibrium is reached at the outlet of the desorption tank. This assumption relies on the gas desorption acceleration by the static mixer followed by a long time of desorption [13].

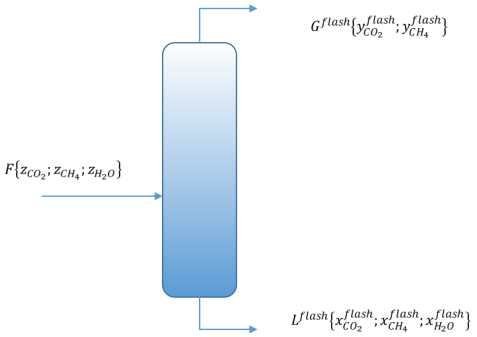

Figure 3: Flash tank flow diagram.

The feed flow entering the flash tank F correspond to the liquid outlet of the HPWS. In this tank, the pressure is around one bar as the gas is released at the atmosphere pressure and gas liquid equilibrium is achieved. Henry's law is used for the carbon dioxide and the methane (Equation (4) and (5)). Molar balance is expressed using Equation (23), (24) and (25) respectively for the global and partials mass balances.

$$F = G^{flash} + L^{flash} \quad (23)$$

$$z_{CH_4}F = y_{CH_4}^{flash} G^{flash} + x_{CH_4}^{flash} L^{flash} \quad (24)$$

$$z_{CO_2}F = y_{CO_2}^{flash} G^{flash} + x_{CO_2}^{flash} L^{flash} \quad (25)$$

By substituting L^{flash} in Equation (24) and (25) using Equation (23), and substituting liquid fraction using Henry's law (Equation (4) and (5)), Equation (24) and (25) can be expressed as Equation (26) and (27).

$$z_{CH_4}F = y_{CH_4}^{flash}G^{flash} + \frac{y_{CH_4}^{flash}}{H_{CH_4}} \cdot (F - G^{flash}) \qquad (26)$$

$$z_{CO_2}F = y_{CO_2}^{flash}G^{flash} + \frac{y_{CO_2}^{flash}}{H_{CO_2}} \cdot (F - G^{flash}) \qquad (27)$$

Gas outlet is supposed to be composed of carbon dioxide and methane only so that Dalton's law is respected: $y_{CO_2}^{flash} + y_{CH_4}^{flash} = 1$. Summing Equation (26) and (27) gives a Rachford-Rice like equation, Equation (28) [40]:

$$\frac{z_{CO_2}F}{G^{flash} + \frac{F - G^{flash}}{H_{CO_2}}} + \frac{z_{CH_4}F}{G^{flash} + \frac{F - G^{flash}}{H_{CH_4}}} = 1 \qquad (28)$$

In equation (28), G^{flash} is the unknown value. It can be calculated using Excel Solver. Then, gas molar fractions are calculated using equation (26) and (27), and liquid molar fraction and liquid flowrate calculated respectively with Henry's law (Equation (4) and (5) and the global molar balance (Equation (1)).

3.4 Numerical resolution

Calculus are conducted on a home-made environment using the Excel solver. Program is separated in two steps using two solvers, to calculate respectively the column outlet that fed the flash regeneration, and the flash regeneration outlet that fed the column. An illustration of the program Framework is provided as an algorithm in Appendix 1. The column resolution uses two variables, liquid fraction of carbon dioxide and methane at the outlet of the column, respectively $x_{CO_2}^0$ and $x_{CH_4}^0$. The known parameters are the gas and liquid inlet in terms of flowrate and composition. Gas outlet composition is given by variation of $x_{CO_2}^0$ and $x_{CH_4}^0$ to comply with the aforementioned imposed conditions (liquid composition at the inlet, given from the flash tank). Solving method is GRG Nonlinear, Precision of 10^{-7}, convergence 10^{-5}, and central derivation is used. The flash resolution uses the gas flow generated by the flash desorption G^{flash} as variable and sum of the gas molar fraction as the objective. Solving method is GRG Nonlinear, Precision of 10-7, convergence of 10-5 and central derivation is used.

A VBA code is implemented to run the program for several iteration. The column resolution starts with a liquid fraction null in carbon dioxide and methane. The liquid outlet fed the flash resolution that provide a new value of liquid fraction. The same path is followed until a steady-state is reached. As presented in Appendix 1, the user has

access to all the process flowrates, compositions, recovery ratio, and also the variation of composition along the packing height.

3.5 Physico-chemical properties

A great number of physico-chemical values are required to be injected in the model developed in this work. Most of them are taken with temperature dependency as it is one of the main parameters for absorption efficiency.

In this model, partition coefficients are assumed to be at infinite dilution in the liquid phase, as carbon dioxide and methane concentrations are low. However, the temperature dependency is considered for both carbon dioxide and methane using the correlation of Holder (1980) Equation (29) to calculate m_i in Pascals [41]. Parameters of Holder's Equation are given in Table 2.

$$m_i = 10^5 \cdot \exp\left(A_i + \frac{B_i}{T}\right) \quad (29)$$

Table 2: Holder's Equation parameters used for carbon dioxide and methane [41].

	Methane	**Carbon dioxide**
A	15.826277	14.2831
B	-1559.0631	-2050.3265

Diffusion coefficient for carbon dioxide and methane in the gas phase are calculated using the correlation of Fuller et al. (1966) Equation (30) [42].

$$D_{CO_2-CH_4} = 0.01 \cdot \frac{T^{1.75} \cdot \left(\frac{1}{M_{CO_2}} + \frac{1}{M_{CH_4}}\right)^{\frac{1}{2}}}{P \cdot \left(V_{CO_2}^{\frac{1}{3}} + V_{CH_4}^{\frac{1}{3}}\right)} \quad (30)$$

V_i is the molar volume of *i* at the boiling point taken from Thibodeaux and Mackay (2011) [43].

Gas viscosity is also calculated considering a mixture of two compound (carbon dioxide and methane). Each compound's viscosity in the gas phase is calculated with temperature dependency according to Sutherland's law Equation (31) [44].

$$\mu(T) = \mu(T_{ref}) \cdot \left(\frac{T}{T_{ref}}\right)^S \quad (31)$$

In equation (31), Temperature of reference T_{ref} is taken at 293 K and corresponding viscosity values are respectively of $1.47 \cdot 10^{-5}$ and $1.1 \cdot 10^{-5}$ Pa·s for carbon dioxide and methane. s is respectively 0.933 and 0.836 for carbon dioxide and methane. Gas viscosity of the mixture is then calculated using correlation of Herning and Zipperer (1936) Equation (32) [45].

$$\mu_g = \frac{(\mu_{CO_2} y_{CO_2} \sqrt{M_{CO_2}} + \mu_{CH_4} y_{CH_4} \sqrt{M_{CH_4}})}{y_{CO_2} \sqrt{M_{CO_2}} + y_{CH_4} \sqrt{M_{CH_4}}} \quad (32)$$

Liquid viscosity μ_L is corrected for temperature using the Equation (33) [34].

$$\mu_L(T) = \alpha \cdot \exp\left(\frac{\beta}{T} + \gamma \cdot T + \delta \cdot T^2\right) \quad (33)$$

Parameters implemented in Equation (33) are presented in Table 3.

Table 3: Parameters for water viscosity correction [34].

	α (mPa.s^{-1})	**β (K)**	**γ (K^{-1})**	**δ (K^{-2})**
Water	$1.856 \cdot 10^{-11}$	4209	0.04527	$-3.376 \cdot 10^{-5}$

Diffusion coefficient in water are also corrected for temperature using Equation (34) from Thibodeaux and MacKay (2011) [43].

$$D_i(T) = D_i(T_{ref}) \cdot \left(\frac{T}{T_{ref}}\right) \cdot \left(\frac{\mu_L(T_{ref})}{\mu_L(T)}\right) \quad (34)$$

In Equation (34), T_{ref} is taken at 298 K and corresponding diffusion coefficient are respectively of $1.92 \cdot 10^{-9}$ and $1.49 \cdot 10^{-9}$ $m^2 \cdot s^{-1}$ for carbon dioxide and methane [46].

4 Results and Discussions

4.1 Model validation

The HPWS developed in this work is validated by comparison to the experimental results obtained by Benizri et al. (2019) using the process presented in the Experimental Methods section of this study [13]. The great number of values are summarized in Appendix 2, with parameters variations in terms of pressure, temperature, gas and liquid flowrates. The results are presented with the elimination rate of carbon dioxide E_{CO_2} and the recovery ratio of methane R_{CH_4} defined using Equation (35) and (36).

$$E_{CO_2} = \frac{y_{CO_2}^{in} - y_{CO_2}^{out}}{y_{CO_2}^{in}} \cdot 100 \quad (35)$$

$$R_{CH_4} = \frac{y_{CH_4}^{out} \cdot G^{out}}{y_{CH_4}^{in} \cdot G^{in}} \cdot 100 \quad (36)$$

First of all, a global mass balance is conducted for both carbon dioxide and methane to confirm that hypothesis do not led to a bias in the modeled results. The relative error (RE) is calculated using Equation (37).

$$RE = \frac{\left(G_i^{in} + L_i^{in}\right) - \left(G_i^{out} + L_i^{out}\right)}{G_i^{in} + L_i^{in}} \cdot 100 \quad (37)$$

RE are calculated for a wide diversity of operating parameters (high differences in liquid flowrate, gas flowrate and pressure) in Table 4 to assess the model validity in various conditions. For all the point simulated, no deviation over 0.5 % was reported for both methane and carbon dioxide. Little relative errors calculated for each point indicate a first validation of the model by mass conservation.

Table 4: Mass balance validation by calculation of the Relative Error for carbon dioxide and methane with four extreme experimental conditions.

Experiment number	Liquid flowrate (m^3/h)	Gas flowrate (Nm^3/h)	P_{Tot} (bars)	RE CO_2	RE CH_4
3	5	16	8.443	0.29	0.016
10	10	24.3	6.433	0.37	0.069
31	10	39.9	8.551	0.46	0.040
39	5	38.4	8.392	0.0038	0.00019

Modelled results are then compared to the experimental results presented in Appendix 2. Figure 4 presents the modeled results obtained with the procedure detailed in the Packing Height section using the numerical resolution presented in Numerical resolution. Results are compared in terms of volumetric gas flowrate at the outlet, G_v^{out} in Figure 4 (a) and in terms of methane purity at the outlet of the column $y_{CH_4}^{out}$ in Figure 4 (b). Volumetric methane flowrate at the outlet G_v^{out,CH_4} is also presented in Figure 4 (c).

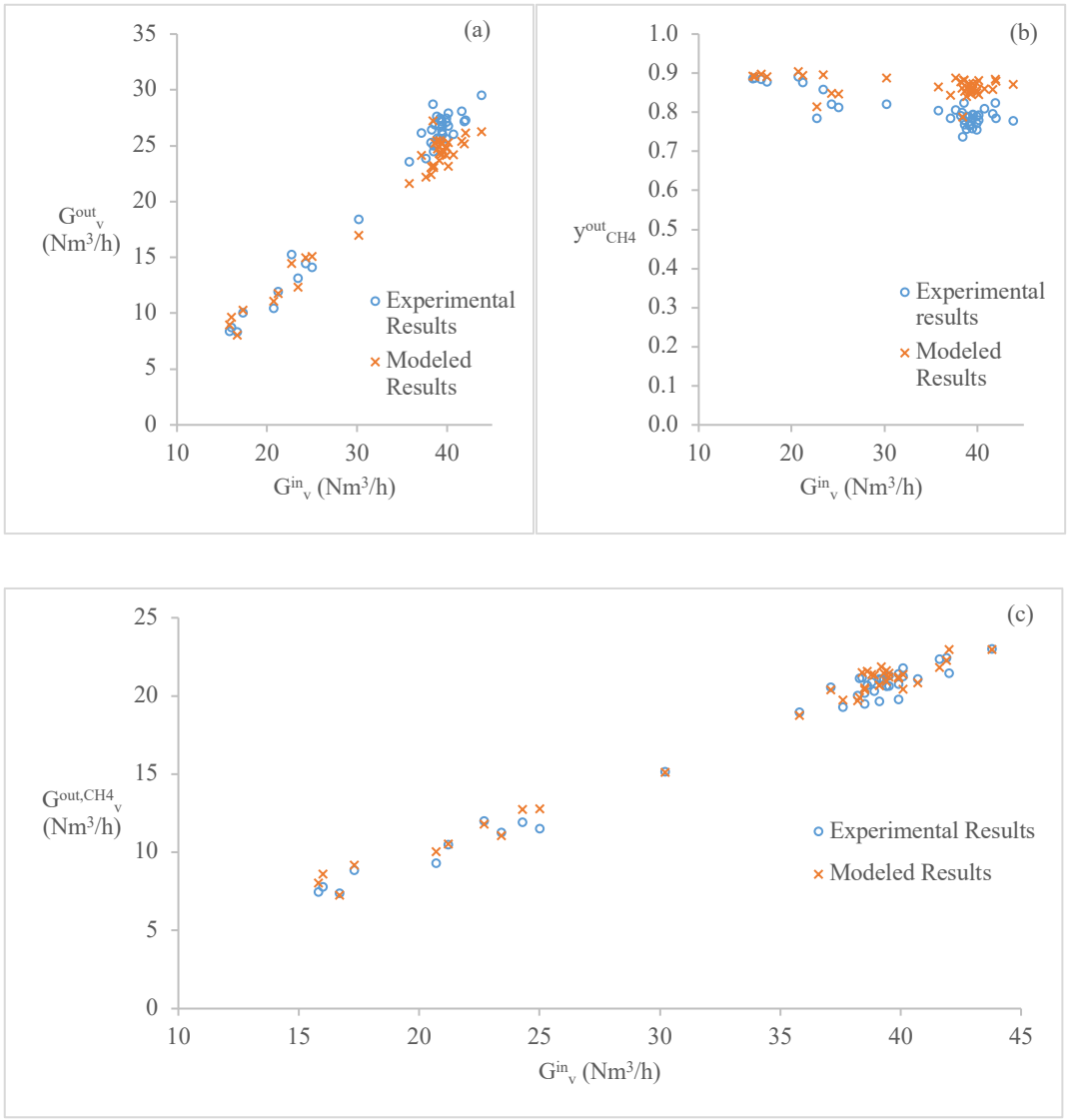

Figure 4: (a) outlet gas flowrate (Nm³/h), (b) outlet molar fraction in methane and (c) outlet methane flowrate obtained by the experiment (Benizri et al. (2019)) [13] in comparison with the simulation.

Figure 4 shows that modeled results are in good agreement with the experimental results obtained by Benizri et al. (2019) [13]. The same trend is observed for both results regarding parameters variations. However, a divergence occurs when increasing G_v^{in} for G_v^{out} and $y_{CH_4}^{out}$ that are respectively underestimated and overestimated. G_v^{out,CH_4} remains well calculated under those circumstances. Those differences might be due to the determination of the volumetric gas flowrate at the outlet by a flowmeter not corrected in pressure for the determination of Normal Cubic Meters. The experimental determination of the volumetric flowrate at the inlet is conducted by a calibration of the speed variation controlling the compressor at atmospheric pressure, leading to a possible bias with the experiments conducted under pressure and so source of uncertainty. Also, this model does not consider any other gas interactions, such as hydrogen sulfide and humidity in the gas, that could modify the final outlet purities.

However, the model considers all the parameters with influences on the mass transfer and successfully transcribes the variation of flowrate along the packing height and the concomitant absorption of the two compounds with no restrictive hypothesis. The model allows to evaluate the variations in the mass transfer and the influences of parameters such as pressure, temperature, liquid and gas flowrates, packing material or the water regeneration. Such a proposal was never proposed in the literature and is of major interest to better understand absorption mechanisms occurring within the HPWS and to optimally operate biogas upgrading.

4.2 Driving forces and mass transfer variation along the column height

Mass transfer in the column is closely linked to the driving forces between the gas and the liquid phases. Those forces are represented by the difference between the fraction of the compound (carbon dioxide or methane) solubilized in the liquid $\left(x_{CO_2}, x_{CH_4}\right)$ and the fraction of the compound that should be solubilized in the liquid if it would be in equilibrium with the gas phase $\left(x^*_{CO_2}, x^*_{CH_4}\right)$. T represents the mass transfer per surface unit across the interface from the gas to the liquid. T is related to x^* and x according to Equation (38) [29].

$$T = K_L^0(x^* - x) \tag{38}$$

If the driving force value $(x^* - x)$ is above zero, the mass transfer occurs from the gas to the liquid. If it is negative, the mass transfer is established in the opposite direction from the liquid to the gas phase.

Figure 5 presents the modeled values of $x^*_{CO_2}, x_{CO_2}, x^*_{CH_4}, x_{CH_4}$ calculated for three operating conditions (low, intermediate, and high inlet gas flowrates). In all the Figures presenting variations with the stage numbers, only one point over four is represented for clarity reason. The volumetric gas flowrates considered are respectively of 15, 30, and 40 Nm^3/h. Other conditions implemented are 10 m^3/h for the liquid flowrate, 9 bars of Pressure in the column, Temperature of 293 K and respective inlet molar fraction of 0.45 and 0.55 for carbon dioxide and methane.

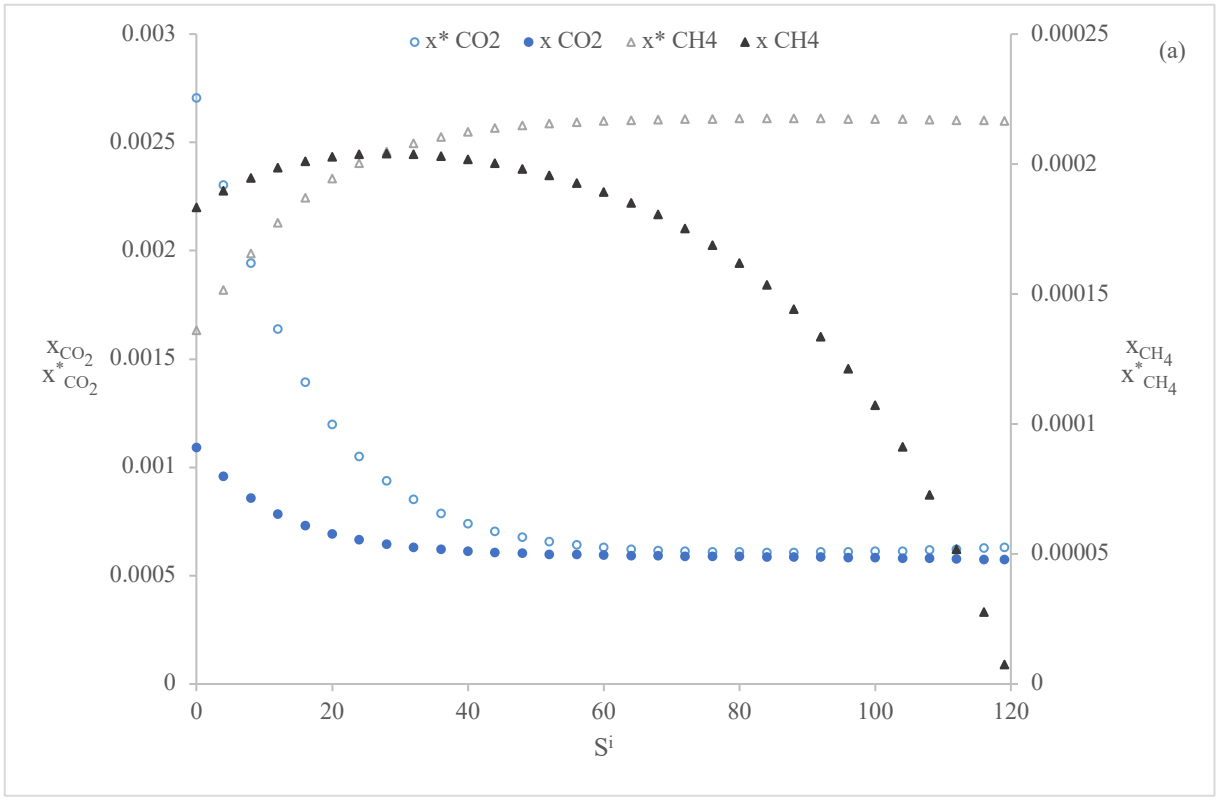
x* CO2
x CO2
x* CH4
x CH4
(a)
0.003
0.0025
0.002
0.0015
0.001
0.0005
0
0.00025
0.0002
0.00015
0.0001
0.00005
0
0
20
40
60
80
100
120
x_{CO_2}
$x^*_{CO_2}$
x_{CH_4}
$x^*_{CH_4}$
S^i

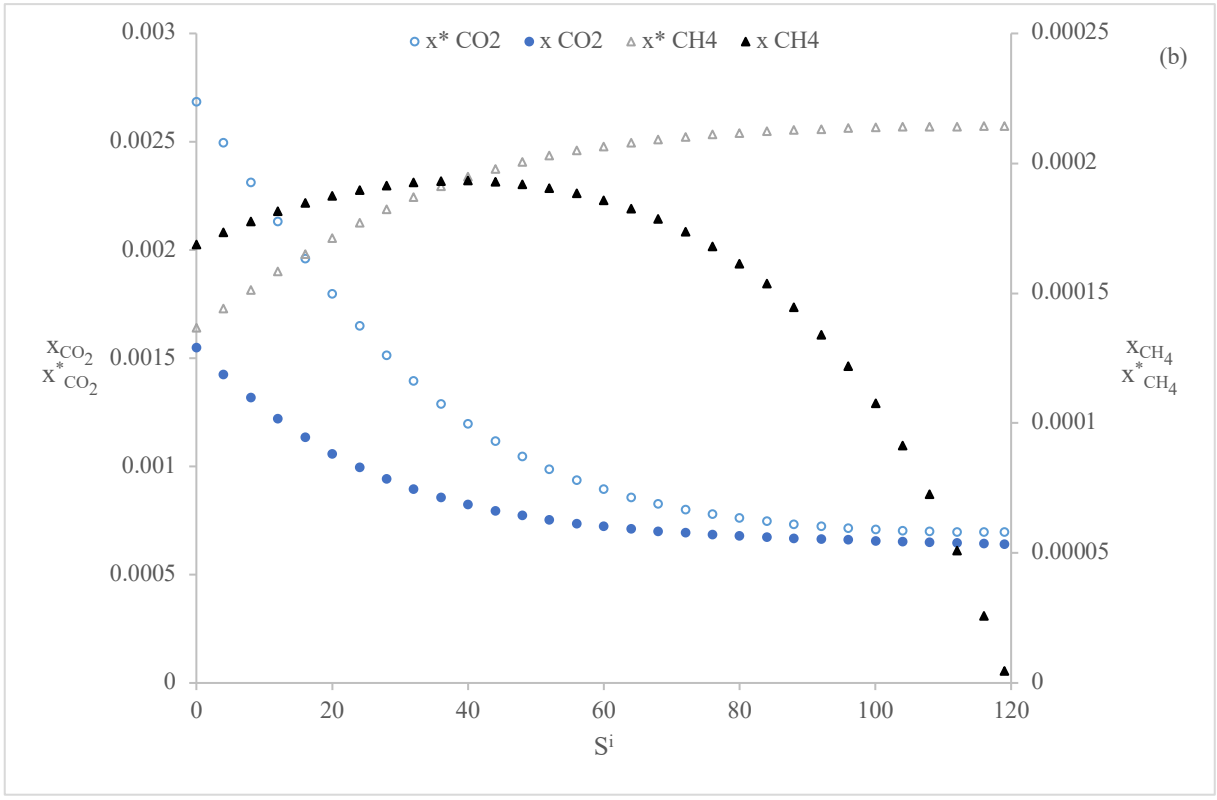
x* CO2
x CO2
x* CH4
x CH4
(b)
0.003
0.0025
0.002
0.0015
0.001
0.0005
0
0.00025
0.0002
0.00015
0.0001
0.00005
0
0
20
40
60
80
100
120
x_{CO_2}
$x^*_{CO_2}$
x_{CH_4}
$x^*_{CH_4}$
S^i

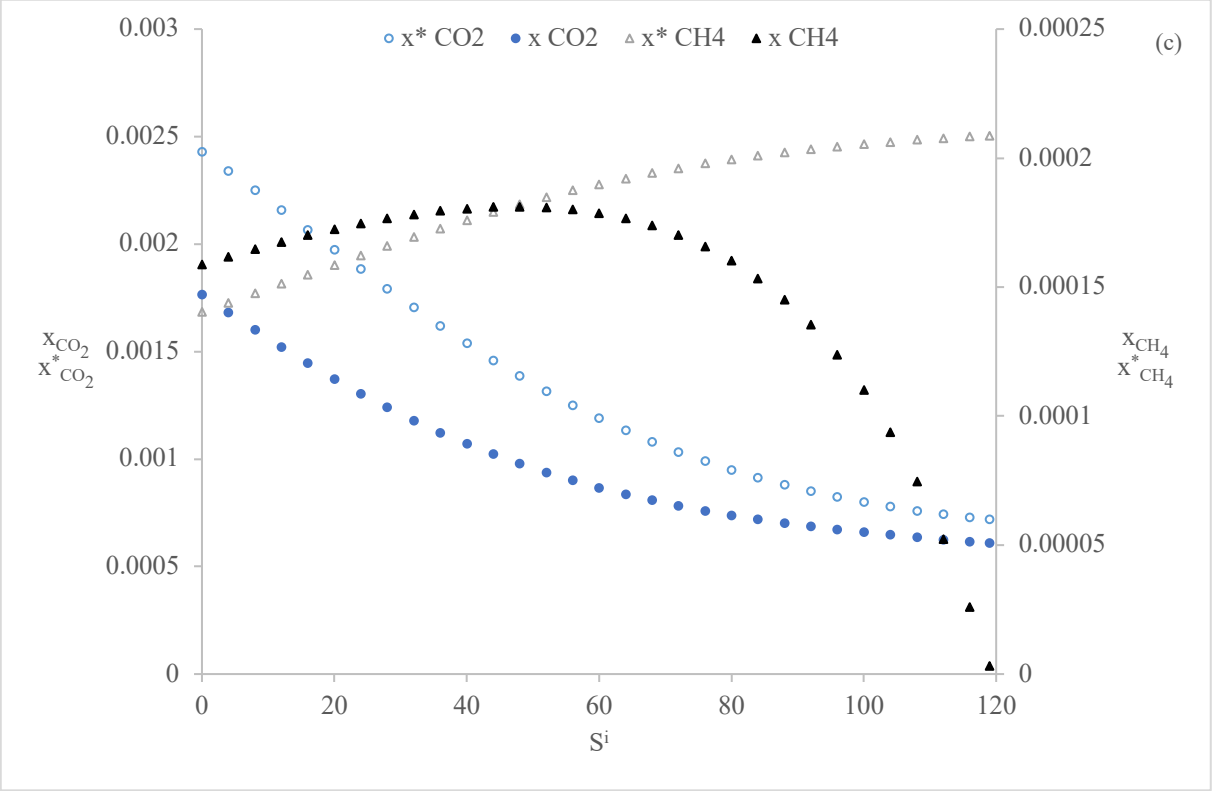

Figure 5: CO_2 and CH_4 liquid molar fraction and liquid molar fraction in equilibrium with the gas phase - Evolution along the packing height represented by the stage number in three conditions: (a) low gas inlet flowrate, (b) intermediate gas inlet flowrate, (c) high gas inlet flowrate.

The three conditions simulated on Figure 5 present a high driving force at the bottom of the column for the carbon dioxide mass transfer from the gas to the liquid. This driving force decreases throughout the packing height until a plateau is reached for cases (a) and (b) representing the equilibrium between the gas and liquid phases. At the highest gas flowrate (c), this plateau is not reached at the top of the column, meaning that the packing height is not sufficient to set the equilibrium in these conditions and that carbon dioxide can still be removed from the gas flow.

For the methane, the evolution is quite surprising with an inversion in the direction of the mass transfer. At the top of the column, when the regenerated water is entering the column, the methane is transferred from the gas to the liquid. But at a certain height of packing (diminishing when reducing the gas flowrate), an intersection point appears below which the methane is desorbed, transferring from the liquid to the gas phase. This mass transfer inversion might be due to the different kinetics of mass transfer for carbon dioxide and methane due to their high difference of solubility in water. It can involve a counter-diffusion phenomenon that diminish the mass transfer between the phases and loosen the transfer of carbon dioxide to the liquid. But it can also be responsible of unexpected methane loss at the liquid outlet, as reported in several studies [15,16]. A fraction of methane still remains in over-saturation at the bottom of the column and does not have enough time to transfer to the gas phase.

4.3 Influence of Pressure and Temperature

Pressure and Temperature are two physical parameters directly affecting phases equilibrium and thus upgrading efficiency. In the experimental device, pressure can be increased up to 10 bars with the compressor. The temperature mostly depends on the weather conditions but can be regulated to a certain extent using a water cooler. A comparison of modeled results between three operating pressures (6 – 8 – 10 bars) at 293 K and three operating temperatures (283 – 293 – 303 K) at 10 bars is presented in Figure 6 to evaluate the impact of those variations on the methane purity and recovery. As maximum targeted gas flowrate is set at 40 Nm^3/h, this condition was implemented along with the maximum liquid flowrate (10 m^3/h) and inlet molar fraction in methane and carbon dioxide respectively of 0.55 and 0.45. Results are presented Figure 6 (a) for Pressure dependency and (b) for Temperature dependency.

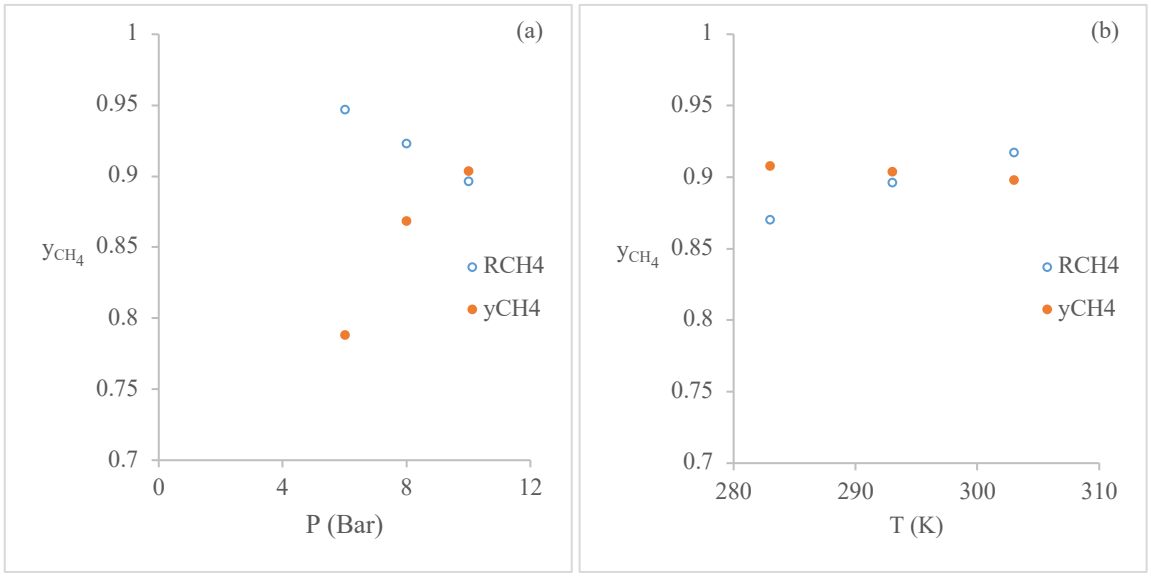

Figure 6: Pressure (a) and Temperature (b) influences on the gas outlet purity and the recovery rate of methane.

Pressure and Temperature both have an influence on the absorption capacity, governing Henry's law and thus the driving force, but also on the hydrodynamics as the volumetric gas flowrate is highly dependent on the Pressure and Temperature conditions. The expected results can be anticipated by an analysis of the equation in the model. As the Pressure increases, volumetric gas flowrate decreases diminishing the k_G value (Equation (18)) and therefore the kinetic of the transfer. But it also promotes a favored equilibrium and a higher driving force (Equation (4), (5) and (10)). And as the Temperature increases, the volumetric flowrate increases rising up the k_G value and the kinetic of the transfer. But the equilibrium is less favored as the Temperature increases because of the Henry's constant, presenting therefore a smaller driving force.

Figure 6 (a) shows a great dependency of $y_{CH_4}^{out}$ and the recovery ratio of the methane with the Pressure. As expected, $y_{CH_4}^{out}$ increases with the Pressure. But a great difference is observed when increasing from 6 to 8 bars compared to 8 to 10 bars. To understand those differences, variations of y_{CH_4} along the column are presented Figure 7 (a) for the three different Pressures. It highlights that at 6 bars, the lowest Pressure considered, the equilibrium is not achieved while it is almost the case at 8 and 10 bars.

Figure 6 shows that the recovery ratio decreases with the Pressure, as more methane is able to transfer from the gas to the liquid and is recover in the liquid outlet. Those results are confirmed in other observations from Kapoor et al. (2017) and Nock et al. (2014) [16,24]. A solution to this methane leaks is to set up an intermediate flash tank to reinject a fraction of the solubilized methane to the column. Anyway, it has to be noted that an excessive Pressure, even if it has a great influence on the methane purity, can be responsible of discriminatory performances as it loosens the recovery of methane and increase the power consumption.

Figure 6 (b) describes a more linear variations for the molar fraction in methane with the Temperature that decreases when the Temperature increases. The recovery rate increases with the Temperature. Variations of y_{CH_4} with the Temperature presented in Figure 7 (b) illustrate not much influence on the outlet methane purity. But those results have to be considered regarding the model configuration, based on a global Temperature on the whole process. Under those conditions, a decrease in the Temperature will improve the absorption capacity, as indicated by Henry's law but also diminish the desorption capacity. So even if the kinetics is faster at low Temperature, it appears that the expected gain in purity is offset by a less effective regeneration of the water at this lower Temperature. To assess this sensitivity, Figure 8 shows the modeled values of y_{CH_4} for three different Temperature in the desorption tank (283 – 288 – 293 K), considering a gas flowrate of 40 Nm^3/h, a Pressure in the column of 10 bars, liquid flowrate of 10 m^3/h and a Temperature of 283 K in the column.

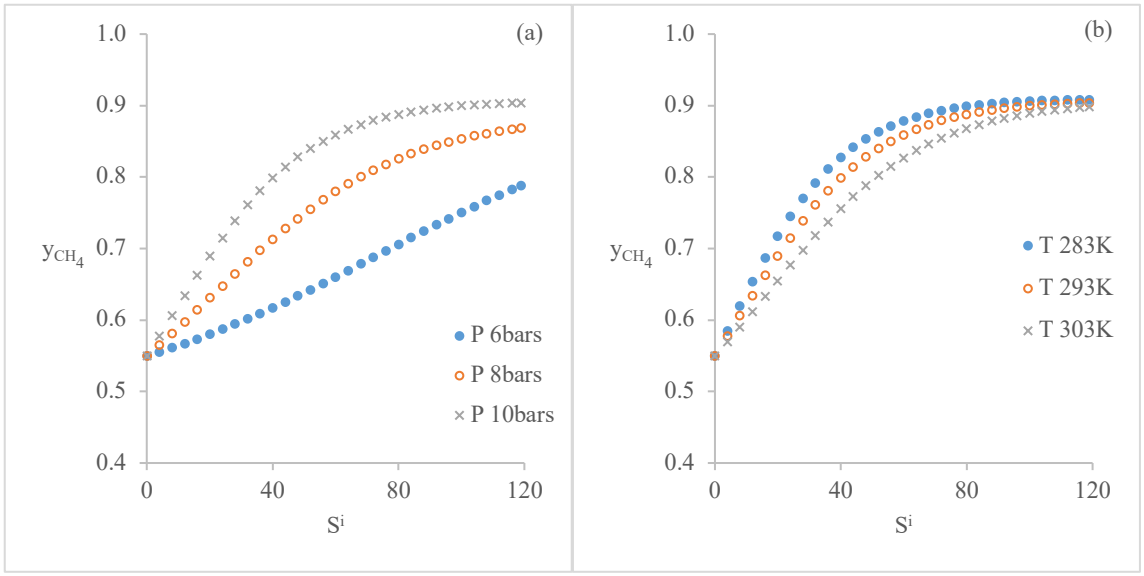

Figure 7: Molar fraction variations of methane in the gas phase along the column for three different Pressures in the column (a) and three different Temperatures (b).

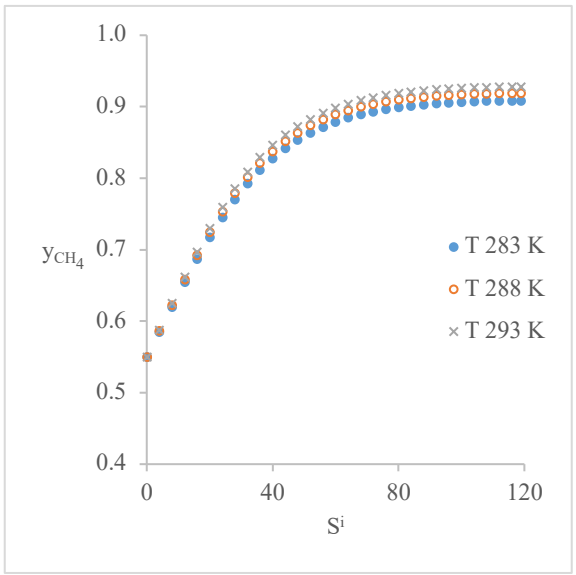

Figure 8: Modeled value of y_{CH_4} along the column for three Temperature of desorption (283 – 288 – 293 K).

Figure 8 highlights the gain on purity by adjusting the Temperature at values suited either for absorption (low Temperature) or for desorption (high Temperature). The recovery ratios calculated under those conditions are stable around 0.90. As on-site process shows increasing Temperature of the liquid phase when running, due to pumping and gas temperature [15], it is a simple and effective way to upgrade the purity of the upgraded biogas without diminishing the recovery ratio. As suggested by Cozma et al. (2013) [25], optimizing the heating phenomenon could be interesting to reduce the energy demand toward the process efficiency. A layout promoting liquid heating in the desorption part and liquid cooling in the absorption part of the process could improve the global performances of the system.

4.4 Influence of liquid-gas ratio

Minimum liquid-gas ratio can be calculated (section Minimum liquid gas ratio) to achieve a desired outlet gas purity supposing that the equilibrium is reached. This supposed to have an infinite column as a contactor and thus this liquid to gas ratio is always taken higher. But as absorption in such a contactor is a dynamic phenomenon, it is not obvious that this equilibrium is reached, and therefore the gas purity might be different than expected. In order to provide a sufficient amount of absorbent, without providing it in excess (that can lead to an increase in the energy consumption with no added value on the gas purity) this liquid to gas ratio is investigated. Figure 9 shows the modeled results of y_{CH_4} along the column height for three operating conditions (6 – 8 – 10 m^3/h). Other conditions implemented are a gas volumetric flowrate of 40 Nm^3/h, a pressure of 10 bars, a Temperature of 283 K and respective molar fraction in methane and carbon dioxide of 0.55 and 0.45.

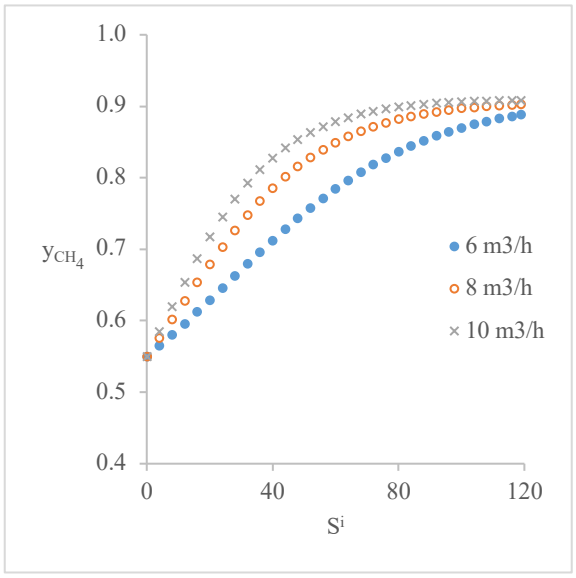

Figure 9: Modeled values of y_{CH_4} along the column for three different liquid flowrates (6 – 8 – 10 m^3/h).

Figure 9 highlights that the mass transfer kinetic is faster for a higher liquid flowrate, and that the equilibrium seems to be established at 8 and 10 m^3/h. But at 6 m^3/h, y_{CH_4} still increases at the bottom of the column, meaning that maximal upgrading capacity is not reached. Those results illustrate that an excess in the liquid flowrate is not always suited to optimal running performances, as it increases the energy consumption with no gain on the gas purity. The mass transfer being increased with the liquid flowrate, rising the liquid flowrate allows to reduce the packing height to reach similar conditions. A techno-economic analysis is recommended to determine the best compromise between investment and operational costs, respectively increased by the column height and by the pumping ratio.

4.5 Influence of packing type

Packing type and packing performances are also of great importance to promote optimal mass transfer between the phases while insuring the best hydrodynamic conditions. Packing manufacturer are focused on improving those mass transfer efficiencies with high loading possibilities. Two different packings are compared in this study. Both are random type and presented in Table 5. They present different characteristics in terms of hydrodynamics and exchange surfaces. RachigSuperRing® can be consider as more hydrodynamically efficient and the second one (Pall Rings) as more mass transfer efficient.

Table 5: Packing characteristics implemented in the model.

Packing Type	**d_P (m)**	**a^* (m^2/m^3)**	**F (m^2/m^3)**	**ε_g**
RaschigSuperRing® (PP)	0.05	205	180	0.93
Pall Ring (PP)	0.016	341	318	0.87

Figure 10 shows the modeled results of y_{CH_4} along the column obtained through the simulations for the two packing materials presented Table 5. Simulations were run implementing the following conditions: Pressure of 8 bars, liquid flowrate of 8 m^3/h, gas flowrate of 40 Nm^3/h, Temperature of 283 K and respective inlet molar fractions of 0.55 and 0.45 in methane and carbon dioxide.

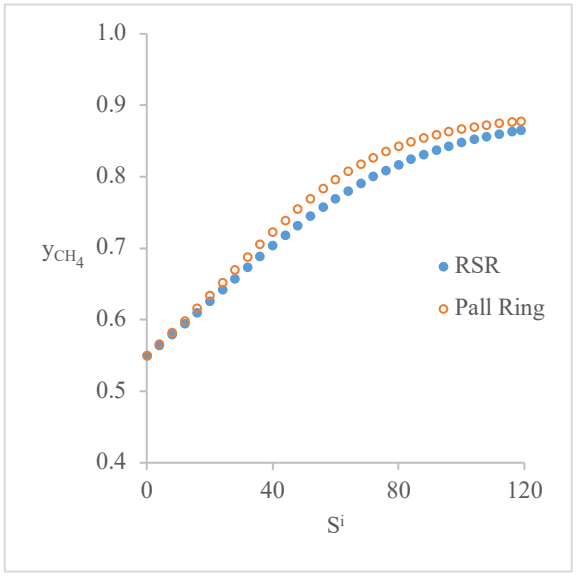

Figure 10: Modeled values of y_{CH_4} along the column for RSR and Pall Ring packings.

Figure 10 illustrates a slightly faster mass transfer when using the Pall Rings presented Table 5 under those conditions than when using the RSR. A smaller packing height can therefore be set with the Pall Rings, but the flooding point also came at smaller gas flowrate allowing less charging capacities. Similarly as for the liquid to

gas ratio, selection of the packing material should be conducted after a techno-economic analysis to highlight the gain of choosing one packing or another.

4.6 Influence of water regeneration

In order to minimize water resource depletion, HPWS are conducted mostly in closed loop on the water involving a regeneration unit to eliminate the dissolved gas in the liquid. Liquid regeneration is usually conducted with a stripping column on large upgrading unit. This technic allows a great regeneration of the absorbent, but came with excessive investment and operating cost that is discriminatory for small anaerobic digester, more suited to the biomass distribution. The regeneration technic presented in Bénizri et al. (2019) and in this work allows a substantial gain by substituting the stripping column with a static mixer and a gas liquid separation. It also allows to retrieve a concentrated flow of carbon dioxide, not diluted in an air stream that is the case in stripping column. In this configuration, carbon dioxide can be easily reused for algae production or for greenhouse cultivation [47–49]. As presented in section Flash tank modeling, this configuration with a static mixer is modeled by a flash tank in equilibrium with the desorbed gas. Desorption possibility is thus limited by the partial pressure of the desorbed gas (mixture of carbone dioxide and methane).

A workaround to this regeneration limitation investigated in this work is to improve the gas desorption thanks to a pressure decrease in the desorption step, the gas being extracted using a rough vacuum pump. In obedience with Henry's law, equilibrium will be displaced to a more favorable value for water regeneration. This possible remedy might be more energetically profitable to reach a high methane purity than running all the powered machine up to their limits, namely for the hydraulic pump (liquid flowrate), the compressor (the column pressure) and the water cooler (the liquid temperature). Figure 11 presents y_{CH_4} variations along the packing height for three different desorption Pressures (0.1 – 0.5 – 1 bar) using running conditions of 40 Nm^3/h for the gas flowrate, 10 bars of Pressure in the column, 10 m^3/h of liquid flowrate, Temperature of 283 K in the column and 288 K for the regeneration. Gas fraction are respectively of 0.55 and 0.45 for methane and carbon dioxide.

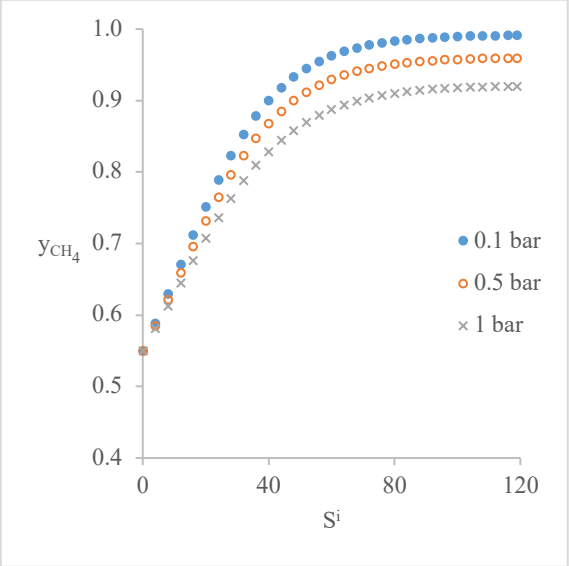

Figure 11: Modeled value of y_{CH_4} along the column for three desorption Pressures (0.1 – 0.5 – 1 bar).

Figure 11 shows a great improvement in both kinetics and final methane purity at the outlet of the column. Outlet purity increases from 0.92 to 0.96 and 0.99 with a desorption Pressure from 1 bar to 0.5 and 0.1 bar. As in other cases the outlet purity in methane is limited to around 0.90 even when powered machines such as the pump and the compressor are run up to their maximums, implementing a rough vacuum in the desorption tank help getting over this barrier and upgrading the methane purity up to the natural gas standards. Besides, recovery ratio of methane calculated under those conditions are respectively of 0.87, 0.865, and 0.86 for the desorption at 1, 0.5 and 0.1 bar. According to the model results, improving the regeneration of the water allows significant enhancement of the methane purity whereas the recovery ratio remains almost unchanged.

4.7 Energy consumption

As underlined all along this work, the purity of the outlet flow and the recovery of methane is related to a certain energy consumption. But many ways exist to obtain the desired objective working on the parameters presented before (such as pressure, temperature, liquid and gas flowrate, or the water regeneration). Each way may not be equivalent to each other and thus an optimal energy consumption can be obtained by using the most suitable parameters. So the whole upgrading process consist of three power engines: the hydraulic pump, the compressor, and the rough vacuum pump. The temperature correction is not considered as it shows little influence on the performances of the process. The energy consumption of those devices depends on a wide number of parameters, but can be estimated regarding the flowrate to circulate and the difference of pressure at the upstream and the downstream of the device. The respective energy consumption ξ is calculated in kWh/Nm^3 of biogas for the hydraulic pump (ξ_{pump}), the compressor (ξ_{comp}) and the vacuum pump (ξ_{vac}) using Equation (39), (40) and (41).

$$\xi_{pump} = \frac{L_v \cdot (P_{col} - P_{flash})}{\eta_{pump} \cdot 1000 \cdot \mathrm{G^{in}}} \quad (39)$$

$$\xi_{comp} = \frac{0.371 \cdot T \cdot \gamma \cdot G_v}{(\gamma - 1) \cdot \eta_{comp} \cdot G^{in}} \left[\left(\frac{P}{P_{Atm}} \right)^{1 - \frac{1}{\gamma}} - 1 \right] \quad (40)$$

$$\xi_{vac} = 3.7 \cdot 10^{-5} \cdot 1.2 \cdot G_v^{flash} \cdot \left(P_{Atm} - P_{flash} \right) \cdot \frac{750}{\mathrm{G^{in}}} \quad (41)$$

In Equation (39), η_{pump} is the pump yield and is taken at 0.6. In Equation (40), γ is the Laplace coefficient of the gas taken at 1.35 and η_{comp} is the compressor yield and is taken at 0.8. In Equation (41), G_v^{flash} is expressed in m^3/h and the pressure are in bars.

The energy consumption is calculated for the three devices by variation of:

- the pressure in the column (8 – 12 – 16 – 20 bars) at a liquid flowrate of 10 m^3/h and a desorption in the flash at atmospheric pressure,
- the liquid flowrate (6 – 8 – 10 – 12 m^3/h) at a pressure of 10 bars and a desorption in the flash at atmospheric pressure,
- and the desorption pressure (1 – 0.5 – 0.2 – 0.1 bar) at a pressure in the column of 10 bars and a liquid flowrate of 10 m^3/h.

In all those simulations, the gas flowrate is set at 40 Nm^3/h, the temperature at 293 K and the inlet molar fraction at 0.45 and 0.55 in carbon dioxide and methane. Optimization calculations are also proposed to reach a gas purity of 0.97. Three points (A, B, C) are presented with respective pressure in the column of 7.6 – 8.5 – 10 bars, liquid flowrate of 8 m^3/h, and a desorption pressure of 0.1 – 0.2 – 0.3 bar. Results are presented in Figure 12.

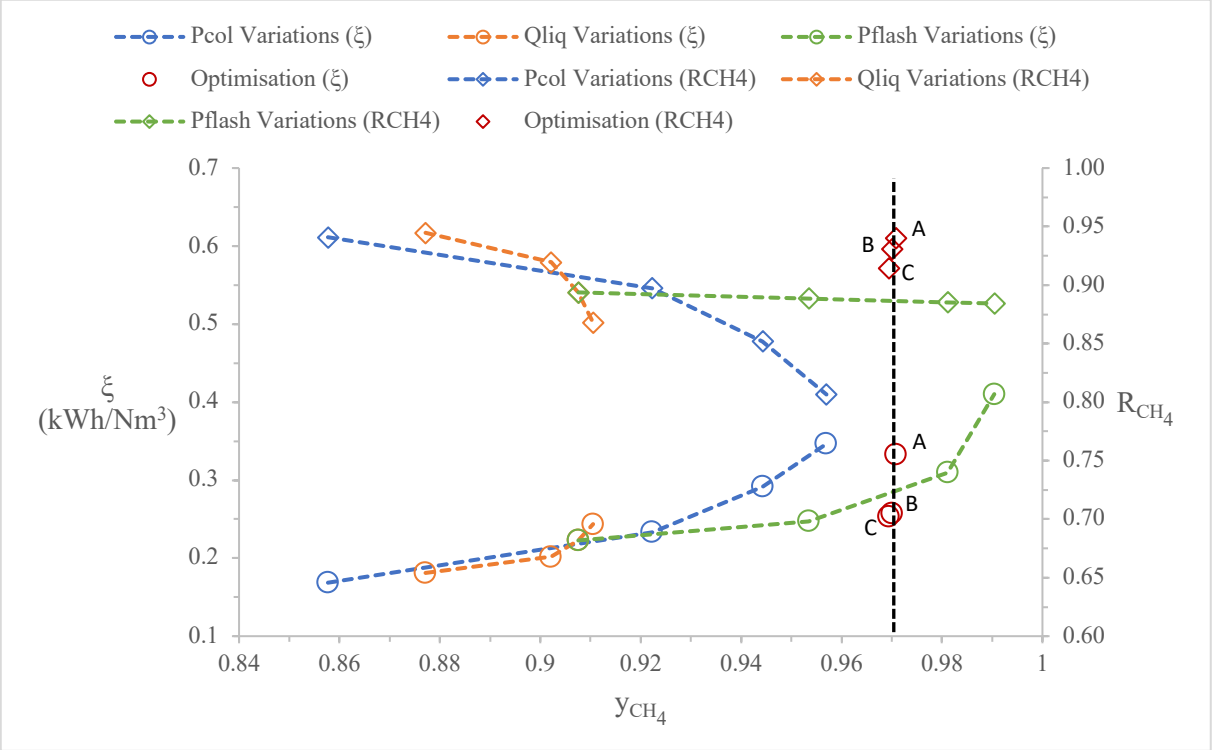

Figure 12: Effects of parameters variations (column pressure, liquid flowrate and desorption pressure) on the methane purity, the energy consumption, and the recovery of methane – Optimization of the operating parameters.

As previously observed, increasing the liquid flowrate allows a great improvement in the methane purity as the equilibrium is reached only for a sufficient flowrate. When it is achieved, a raise in the liquid flowrate is only associated to a waste of energy and a loss in methane with no significant improvement in the methane purity. The liquid flowrate has to be chosen with great attention as it can hinder the process performances pointlessly. Increasing the pressure in the column also allows to significantly improve the methane purity. But it is also associated to a substantial loss in methane and a growing demand in energy that can not meet the gas standards over 97 % in methane with viable performances. Also, a pressurized vessel is associated to restrictive standards in the manufacturing and the operating in most countries. A high-pressured column could be also difficult to set up on agricultural environment. Concerning the pressure decrease in the flash tank obtained by the rough vacuum pump, the same trend appears in the energy consumption with a high increase for not much gain in methane purity, but it is shifted to a more favorable methane purity with similar energy consumption. Implementing this parameter in the process allows to significantly improve the methane purity with similar energy consumption and a methane recovery much higher than by setting excessive value of pressure and liquid flowrate. Optimization estimations were conducted to underline that different paths allow to reach a targeted value of methane purity (0.97 in this case) with very different performances of the HPWS. It appears that in this particular case, a flash pressure of 0.2 bar is the most suited value. With a pressure of 0.1 bar, the power requirement is detrimental (0.33 kWh/Nm^3

compared to 0.25 kWh/Nm^3) while a pressure of 0.3 bar is similar in terms of power requirement but is associated to more methane loss (0.91 compare to 0.93 for the recovery ratio). The main conclusion that is brought out from those power requirement estimations is that for the three parameters targeted (pressure in the column, liquid flowrate, and pressure in the flash tank), they should not be raised in excess insofar as it is associated to an increase in the energy consumption and detrimental performances. However, implementing a rough vacuum in the flash tank to improve the water regeneration and its absorption performances would break the technological limitations that hold HPWS for small-scale applications under the gas standards.

5 Conclusions

A rate-based model was developed for High Pressure Water Scrubbing considering the decrease of gas flowrate observed along the packing height and the simultaneous absorption of several component (carbon dioxide and methane). Those conditions notably occur in biogas upgrading, that were selected for model validation. The model is based on a subdivision of the column height in a certain number of stages where the Transfer Unit method is applied. Variations in terms of flowrate and molar fraction in the gas and the liquid are calculated all along the packing height. This allows to better understand the mechanisms occurring in a HPWS and to optimize the operating parameters of a running process.

The model was validated by comparison with experimental data recovered on a farm plant with a configuration similar to the model. Model results and experimental results are close to each other regarding the methane purity and the gas flowrate at the outlet of the column.

Operating and chemicophysical parameters influence on the process performances were evaluated in terms of methane purity and methane recovery. It is possible to reach a targeted purity in methane associated to a certain recovery ratio working on several aspect: Pressure, Temperature, Liquid-Gas ratio, Packing material, and the water regeneration. Modeled results illustrate that all parameters have an impact on the process efficiency, modifying the theoretical reachable $y_{CH_4}^{out}$ and recovery ratio, but also on the needed height of packing to complete the mass transfer. While some parameters only have influence on the mass transfer kinetics (liquid-gas ratio if above the minimum liquid-gas ratio required to reach the equilibrium and the packing material), others like the Pressure, the Temperature and the water regeneration have influences on both the final theoretical methane purity and recovery ratio and the mass transfer kinetics. Pressure increase allows to significantly improve the methane purity but it also favored methane loss. Temperature has less influence on the performances, but simple layout of the process can

upgrade methane purity with not much difficulty and energy consumption. Water regeneration presents the prevailing influence on the process performances. Desorption conducted at 0.1 bar of rough vacuum rather than 1 bar enable to enhance the methane purity from 90 % up to 99 % with a similar recovery ratio of 87 %. If a purity of 0.97 is targeted, the model suggests a desorption pressure of 0.2 bar to minimize the energy consumption while maximizing the recovery of methane. This configuration, associated to an intermediate pressured flash vessel to recover a high fraction of methane, could significantly improve the methane purity with a high recovery rate of methane and a low energy consumption. In this way, energy return on investment is optimized and financial viability of biogas upgrading at small scale can be reached.

Those results underline the necessity of rate-based modeling considering hydrodynamics' influence on mass-transfer as HPWS are dynamic processes with significant dependences toward operating parameters.

Acknowledgments

The authors are very grateful to the French Environment and Energy Management Agency (ADEME) for the founding support provided within the EPUROGAZ grant.

References

[1] V. Smil, Energy and Civilization: A History, The MIT Press, Cambridge, 2017.

[2] V. Masson Delmotte, P. Zhai, H.-O. Pörtner, Summary for Policymakers — Global Warming of 1.5 ºC, IPCC, World Meteorological Organization, Switzerland, 2018.

[3] V. Smil, Energy Transitions: History, Requirements, Prospects, Praeger, ABC-CLIO, LLC, Santa Barbara, 2010.

[4] E. Ottmar, R.P. Madruga, Y. Sokona, Renewable energy sources and climate change mitigation: special report of the Intergovernmental Panel on Climate Change, Cambridge University Press, New York, 2012.

[5] U. Brémond, A. Bertrandias, J.-P. Steyer, N. Bernet, H. Carrere, A vision of European biogas sector development towards 2030: Trends and challenges, Journal of Cleaner Production. 287 (2021) 125065. https://doi.org/10.1016/j.jclepro.2020.125065.

[6] R. Moletta, La méthanisation, Tec&Doc, Lavoisier, Paris, 2015.

[7] A. Rafiee, K.R. Khalilpour, J. Prest, I. Skryabin, Biogas as an energy vector, Biomass and Bioenergy. 144 (2021) 105935. https://doi.org/10.1016/j.biombioe.2020.105935.

[8] S. O'Connor, E. Ehimen, S.C. Pillai, A. Black, D. Tormey, J. Bartlett, Biogas production from small-scale anaerobic digestion plants on European farms, Renewable and Sustainable Energy Reviews. 139 (2021) 110580. https://doi.org/10.1016/j.rser.2020.110580.

[9] N. Scarlat, J.-F. Dallemand, F. Fahl, Biogas: Developments and perspectives in Europe, Renewable Energy. 129 (2018) 457–472. https://doi.org/10.1016/j.renene.2018.03.006.

[10] F. Ardolino, G.F. Cardamone, F. Parrillo, U. Arena, Biogas-to-biomethane upgrading: A comparative review and assessment in a life cycle perspective, Renewable and Sustainable Energy Reviews. 139 (2021) 110588. https://doi.org/10.1016/j.rser.2020.110588.

[11] I. Angelidaki, L. Treu, P. Tsapekos, G. Luo, S. Campanaro, H. Wenzel, P.G. Kougias, Biogas upgrading and utilization: Current status and perspectives, Biotechnology Advances. 36 (2018) 452–466. https://doi.org/10.1016/j.biotechadv.2018.01.011.

[12] Q. Sun, H. Li, J. Yan, L. Liu, Z. Yu, X. Yu, Selection of appropriate biogas upgrading technology-a review of biogas cleaning, upgrading and utilisation, Renewable and Sustainable Energy Reviews. 51 (2015) 521–532. https://doi.org/10.1016/j.rser.2015.06.029.

[13] D. Benizri, N. Dietrich, P. Labeyrie, G. Hébrard, A compact, economic scrubber to improve farm biogas upgrading systems, Separation and Purification Technology. 219 (2019) 169–179. https://doi.org/10.1016/j.seppur.2019.02.054.

[14] S. Sahota, G. Shah, P. Ghosh, R. Kapoor, S. Sengupta, P. Singh, V. Vijay, A. Sahay, V.K. Vijay, I.S. Thakur, Review of trends in biogas upgradation technologies and future perspectives, Bioresource Technology Reports. 1 (2018) 79–88. https://doi.org/10.1016/j.biteb.2018.01.002.

[15] D. Benizri, Epuration du biogaz à la ferme : EPUROGAS, une solution énergétique et économique d'avenir. Etude expérimentale et modélisation d'un procédé d'absorption de dioxyde de carbone avec de l'eau sous pression à une échelle industrielle, Université de Toulouse, 2016.

[16] R. Kapoor, P.M.V. Subbarao, V.K. Vijay, G. Shah, S. Sahota, D. Singh, M. Verma, Factors affecting methane loss from a water scrubbing based biogas upgrading system, Applied Energy. 208 (2017) 1379–1388. https://doi.org/10.1016/j.apenergy.2017.09.017.

[17] H. Wang, C. Ma, Z. Yang, X. Lu, X. Ji, Improving high-pressure water scrubbing through process integration and solvent selection for biogas upgrading, Applied Energy. 276 (2020) 115462. https://doi.org/10.1016/j.apenergy.2020.115462.

[18] M. Pöschl, S. Ward, P. Owende, Evaluation of energy efficiency of various biogas production and utilization pathways, Applied Energy. 87 (2010) 3305–3321. https://doi.org/10.1016/j.apenergy.2010.05.011.

[19] L. Lombardi, G. Francini, Techno-economic and environmental assessment of the main biogas upgrading technologies, Renewable Energy. 156 (2020) 440–458. https://doi.org/10.1016/j.renene.2020.04.083.

[20] C.E. Wylock, W.M. Budzianowski, Performance evaluation of biogas upgrading by pressurized water scrubbing via modelling and simulation, Chemical Engineering Science. 170 (2017) 639–652. https://doi.org/10.1016/j.ces.2017.01.012.

[21] M. Miltner, A. Makaruk, M. Harasek, Review on available biogas upgrading technologies and innovations towards advanced solutions, Journal of Cleaner Production. 161 (2017) 1329–1337. https://doi.org/10.1016/j.jclepro.2017.06.045.

[22] S. Rasi, J. Läntelä, J. Rintala, Upgrading landfill gas using a high pressure water absorption process, Fuel. 115 (2014) 539–543. https://doi.org/10.1016/j.fuel.2013.07.082.

[23] S.A. Hosseinipour, M. Mehrpooya, Comparison of the biogas upgrading methods as a transportation fuel, Renewable Energy. 130 (2019) 641–655. https://doi.org/10.1016/j.renene.2018.06.089.

[24] W.J. Nock, M. Walker, R. Kapoor, S. Heaven, Modeling the Water Scrubbing Process and Energy Requirements for CO2 Capture to Upgrade Biogas to Biomethane, Ind. Eng. Chem. Res. 53 (2014) 12783–12792. https://doi.org/10.1021/ie501280p.

[25] P. Cozma, C. Ghinea, I. Mămăligă, W. Wukovits, A. Friedl, M. Gavrilescu, Environmental Impact Assessment of High Pressure Water Scrubbing Biogas Upgrading Technology, CLEAN – Soil, Air, Water. 41 (2013) 917–927. https://doi.org/10.1002/clen.201200303.

[26] P. Cozma, W. Wukovits, I. Mămăligă, A. Friedl, M. Gavrilescu, Modeling and simulation of high pressure water scrubbing technology applied for biogas upgrading, Clean Technologies and Environmental Policy. 17 (2014) 373–391. https://doi.org/10.1007/s10098-014-0787-7.

[27] J. Läntelä, S. Rasi, J. Lehtinen, J. Rintala, Landfill gas upgrading with pilot-scale water scrubber: Performance assessment with absorption water recycling, Applied Energy. 92 (2012) 307–314. https://doi.org/10.1016/j.apenergy.2011.10.011.

[28] R. Kapoor, P. Ghosh, M. Kumar, V.K. Vijay, Evaluation of biogas upgrading technologies and future perspectives: a review, Environ Sci Pollut Res. 26 (2019) 11631–11661. https://doi.org/10.1007/s11356-019-04767-1.

[29] M. Roustan, Transferts gaz-liquide dans les procédés de traitement des eaux et des effluents gazeux, Tec&Doc, Lavoisier, Paris, 2003.

[30] W.L. McCabe, J.C. Smith, P. Harriott, Unit Operations of Chemical Engineering, McGraw-Hill, 1993.

[31] G. Hebrard, D. Benizri, P. Labeyrie, N. Dietrich, Device for Separating Gas Components Contained in a Gas Mixture, and Use Thereof for Separating Methane and Carbon Dioxide from a Biogas, EP3116626 (A1), 2017.

[32] G. Hebrard, Device, useful in an installation for recovery of methane and carbon dioxide from liquid and biogas under pressure, comprises a degassing tank, a degassing unit, and a reservoir containing a pressurized liquid, FR2972643 (A1), 2012.

[33] C. Ma, C. Liu, X. Lu, X. Ji, Techno-economic analysis and performance comparison of aqueous deep eutectic solvent and other physical absorbents for biogas upgrading, Applied Energy. 225 (2018) 437–447. https://doi.org/10.1016/j.apenergy.2018.04.112.

[34] R.C. Reid, T.K. Sherwood, J.M. Prausnitz, B.E. Poling, B.E. Poling, The Properties of Gases and Liquids, McGraw-Hill, 1987.

[35] L. Sigg, P. Behra, W. Stumm, Chimie des milieux aquatiques, Dunod, 2014.

[36] J.-P. Couderc, C. Gourdon, A. Liné, Phénomènes de transfert en génie des procédés, Tec&Doc, Lavoisier, 2008.

[37] W.K. Lewis, W.G. Whitman, Principles of Gas Absorption., Ind. Eng. Chem. 16 (1924) 1215–1220. https://doi.org/10.1021/ie50180a002.

[38] K. Onda, H. Takeuchi, Y. Okumoto, Mass Transfer Coefficients Between Gas and Liquid Phases in Packed Columns, Journal of Chemical Engineering of Japan. 1 (1968) 56–62. https://doi.org/10.1252/jcej.1.56.

[39] T.K. Sherwood, R.L. Pigford, C.R. Wilke, Mass transfer, Mcgraw-Hill, New York, 1975.

[40] Y. Li, R.T. Johns, K. Ahmadi, A rapid and robust alternative to Rachford–Rice in flash calculations, Fluid Phase Equilibria. 316 (2012) 85–97. https://doi.org/10.1016/j.fluid.2011.12.005.

[41] G.D. Holder, G. Corbin, K.D. Papadopoulos, Thermodynamic and Molecular Properties of Gas Hydrates from Mixtures Containing Methane, Argon, and Krypton, Ind. Eng. Chem. Fundam. 19 (1980) 282–286. https://doi.org/10.1021/i160075a008.

[42] E.N. Fuller, P.D. Schettler, J.C. Giddings, A new method for prediction of binary gas-phase diffusion coefficients, Industrial and Engineering Chemistry. 58 (1966) 18–27. https://doi.org/10.1021/ie50677a007.

[43] L.J. Thibodeaux, D. Mackay, Handbook of Chemical Mass Transport in the Environment, CRC Press, Boca Raton, 2010.

[44] W.M. Haynes, CRC Handbook of Chemistry and Physics, CRC Press, 2014.

[45] N.L. Carr, R. Kobayashi, D.B. Burrows, Viscosity of Hydrocarbon Gases Under Pressure, Journal of Petroleum Technology. 6 (1954) 47–55. https://doi.org/10.2118/297-g.

[46] E.L. Cussler, Diffusion: Mass transfer in fluid systems, Cambridge University Press, New York, 1997.

[47] X. Wang, E. Nordlander, E. Thorin, J. Yan, Microalgal biomethane production integrated with an existing biogas plant: A case study in Sweden, Applied Energy. 112 (2013) 478–484. https://doi.org/10.1016/j.apenergy.2013.04.087.

[48] R. Porcelli, F. Dotto, L. Pezzolesi, D. Marazza, N. Greggio, S. Righi, Comparative life cycle assessment of microalgae cultivation for non-energy purposes using different carbon dioxide sources, Science of The Total Environment. 721 (2020) 137714. https://doi.org/10.1016/j.scitotenv.2020.137714.

[49] Y. Li, Y. Ding, D. Li, Z. Miao, Automatic carbon dioxide enrichment strategies in the greenhouse: A review, Biosystems Engineering. 171 (2018) 101–119. https://doi.org/10.1016/j.biosystemseng.2018.04.018.

Symbols

Generals

a^*	Wetted surface area ($m^2.m^{-3}$)
a^0	Area of interface per unit packed volume ($m^2.m^{-3}$)
A	Absorption factor
D	Diffusion coefficient ($m^2.s^{-1}$)
d_p	Diameter of a packing unit (m)
F	Packing Factor ($m^2.m^{-3}$)
G	Gas molar flowrate ($mol.s^{-1}$)
G_v	Gas volumetric flowrate ($m^3.s^{-1}$)
H	Henry's coefficient (dimensionless)
HUT	Height of a Unit Transfer (m)
K_G^0	Overall gas phase transfer coefficient ($kmol.m^{-2}.s^{-1}$)
k^0	Local mass transfer coefficient ($kmol.m^{-2}.s^{-1}$)
k	Local mass transfer coefficient ($m.s^{-1}$)
L	Liquid molar flowrate ($mol.s^{-1}$)
L_M	Liquid mass flowrate ($kg.m^{-2}.s^{-1}$)
m	Henry's coefficient (Pa)
M	Molecular weight ($kg.mol^{-1}$)
NUT	Number of Unit Transfer
P	Absolute Pressure (Pa)
RE	Relative Error
S^i	Stage i
T	Temperature (K)

x	Molar fraction of solute in liquid
y	Molar fraction of solute in gas
$Z/z^{(i)}$	Height of Total packing / Stage (i) (m)

Subscripts and Superscripts

col	Related to the column
comp	Refers to the compressor
flash	Related to the flash
(i)	Refers to stage (i)
in	Inlet
out	Outlet
G	Refers to the gas phase
j,k	Refers to compound j or k
L	Refers to the liquid phase
M	Mass
pump	Refers to the hydraulic pump
vac	Refers to the vacuum pump
*	In equilibrium with the other phase

Greek Letter

γ	Laplace coefficient
ε	Packing Void ratio
η	Power device yield
μ	Viscosity (Pa.s)

ξ	Energy consumption (kWh/Nm^3)
ρ	Volumetric mass density (kg.m^{-3})
σ	Surface tension (N.m^{-1})
Ω	Cross sectional area of the column (m^2)

Dimensionless Numbers

Ga	$\frac{g d_p^3 \rho^2}{\mu^2}$
Re	$\frac{U d_p \rho}{\mu}$
Sc	$\frac{\mu}{\rho D}$
Sh	$\frac{k d_p}{D}$
We	$\frac{d_p L_M^2}{\rho_L \sigma_L}$

Appendix 1. Programm Algorithm

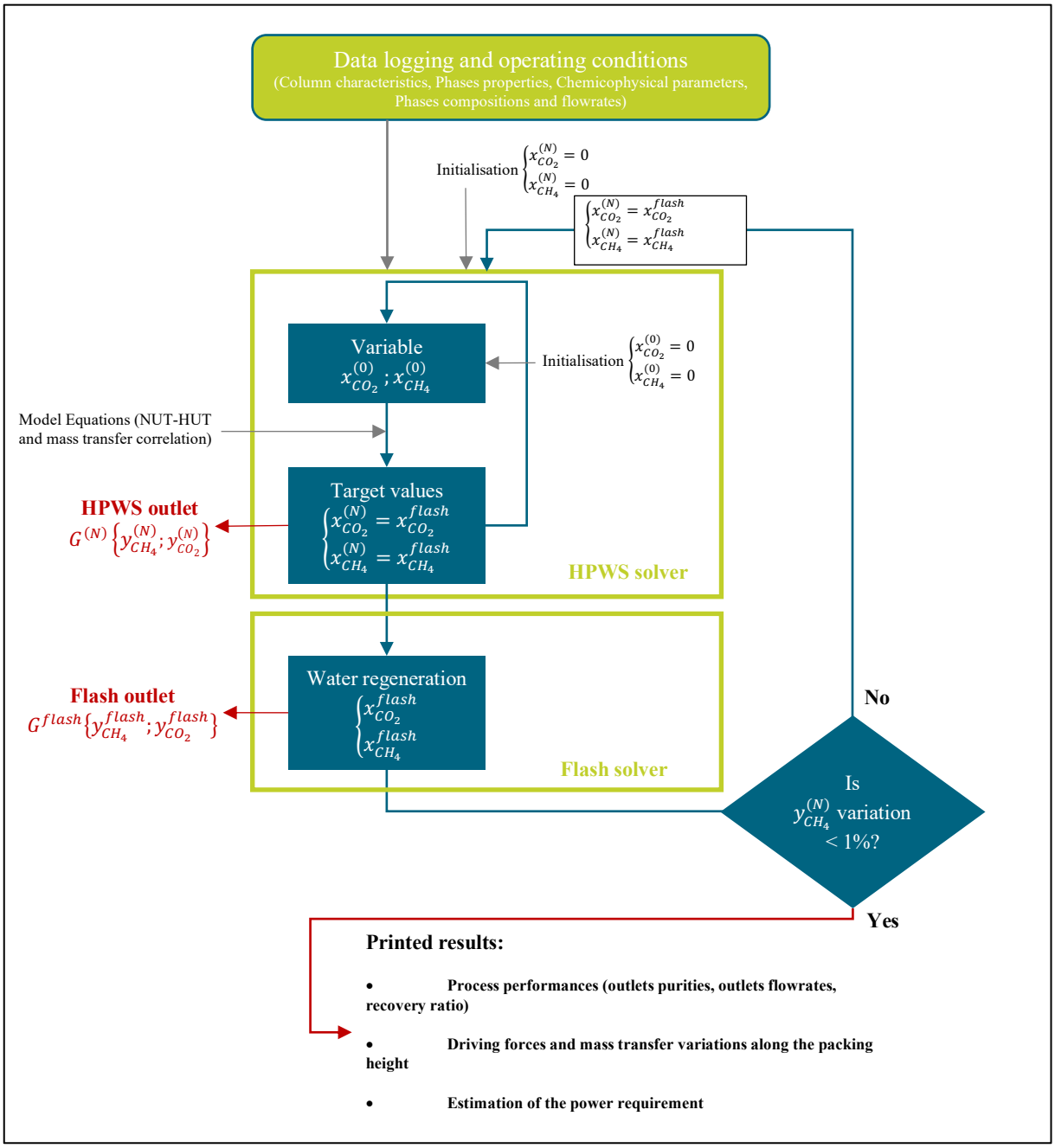

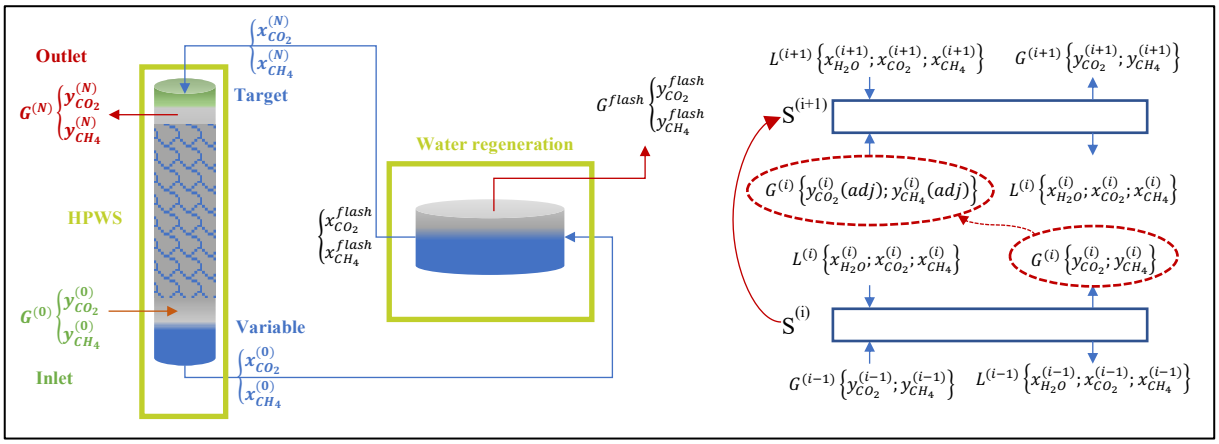

Appendix 2. Experimental results from Benizri et al. (2019)

Experiment number	Liquid flowrate (m^3/h)	Gas Flowrate (Nm^3/h)	P_{CO_2} (bars)	P_{CH_4} (bars)	T (K)	E_{CO_2}	R_{CH_4}
1	10	20.7	3.771	5.2	299.5	74	77.5
2	9.979	16.7	3.514	4.544	288.2	73.7	78.4
3	5	16	3.371	5.072	292.9	72.1	80.9
4	7.5	15.8	3.173	4.774	292.9	71.4	78.3
5	5	17.3	3.729	5.142	301.6	71.2	88.2
6	10	21.2	3.52	4.854	300.1	70.8	85.3
7	9.989	23.4	3.622	4.732	288.4	67.2	85
8	9.841	30.2	3.544	4.629	288.9	58.8	88.4
9	9.19	41.9	3.609	5.003	284.6	58.2	92.1
10	10	24.3	2.744	3.689	301.1	58.1	85.3
11	9.283	38.5	3.438	4.818	283.3	57.7	89.7
12	10	25	2.847	3.601	301.1	57.5	82.3
12	8.243	40.7	3.557	4.367	285.2	57.5	93.9
13	9.439	35.8	3.24	4.275	289.7	54.5	93
14	9.939	37.6	3.599	4.944	289.4	54.1	88.5
15	9.374	40.1	3.232	4.027	288.4	53.5	95.5
16	9.306	38.3	3.143	4.138	281.9	53.5	97
17	8.535	41.6	3.453	4.449	287.2	53.2	95.4
18	9.83	38.2	3.548	4.634	289.6	52	92.5
19	8.783	39.9	3.301	4.31	290.7	51.6	94.8
20	9.361	39.5	3.207	4.395	289.5	51.5	93.2
21	8.867	39.1	3.224	4.21	289.6	51	95.2
22	10	22.7	2.291	2.981	294.9	50.3	93.4
23	9.45	39.5	3.345	4.791	290.4	49.5	88.7
24	8.702	40.1	3.356	4.382	294.4	49.3	95.9
25	9.927	39.4	3.262	4.388	291.6	49.2	91.2
26	9.869	43.8	3.603	4.706	290.2	48.9	92.7
27	9.914	38.9	3.098	4.488	291.7	48.5	88.1
28	9.739	37.1	3.11	4.374	302.4	48.3	94.7
29	9.86	38.5	3.616	4.958	296.1	47.8	87.5
30	9.666	42	3.513	5.09	292.6	47.4	86.3
31	10.001	39.9	3.672	4.879	299.2	46.9	86.9
32	9.829	39.1	3.598	4.781	297.7	45.7	88.1
33	9.863	39.3	3.244	4.478	301.7	44.8	92.2
34	9.677	39.9	3.432	4.511	298.5	43.4	91.5
35	6.931	38.6	3.409	4.939	290.8	43.2	90.5
36	6.934	39.2	3.471	5.03	290	42.9	90.9
37	10.009	39.4	3.355	4.719	303.4	42	89.6
38	7.098	38.8	3.376	4.698	292.6	41.7	92.5
39	5.034	38.4	3.509	4.883	292.6	37.1	94.7